THE ASTRONOMICAL JOURNAL VOLUME 97, NUMBER 6 JUNE 1989

A CCD PORTRAIT OF COMET P/TEMPEL 2[a]

DAVID JEWITT
Institute for Astronomy, University of Hawaii, 2680 Woodlawn Drive, Honolulu, Hawaii 96822

JANE LUU
Department of Earth, Atmospheric, and Planetary Sciences, Massachusetts Institute of Technology, Cambridge, Massachusetts 02139
Received 29 December 1988; revised 19 February 1989

ABSTRACT

The development of activity in comet P/Tempel 2 is studied from aphelion ($R = 4$ AU) to perihelion ($R = 1.4$ AU) using extensive time-series charge-coupled device (CCD) photometry and CCD spectra. The comet undergoes a profound morphological change at $R \approx 2$–2.5 AU, from a bare nucleus at larger distances to an active comet supporting a coma of gas and dust. Cyclic photometric variations with the period $T = 8.95 \pm 0.01$ hr are present at all R, and are attributed to the rotation of the nucleus at this period. The nucleus is prolate (axes $a{:}b{:}c = 1.9{:}1{:}1$), a property shared with other nuclei studied using CCD photometry. Novel results include a limit on the bulk density of the nucleus, $\rho \geqslant 300$ kg m^{-3}, and a 20-Å-resolution CCD spectrum of the nucleus. Spatially and temporally resolved photometry is used to study the effects of nucleus rotation on the coma. The coma does not share the dramatic photometric variations shown by the nucleus. It possesses a steep surface-brightness distribution, which we attribute to progressive destruction of the coma grains with increasing space exposure.

I. INTRODUCTION

Recent ground-based observations taken using charge-coupled device (CCD) detectors have revealed the physical properties of the nuclei of several comets. The nuclei of comets Arend–Rigaux, Neujmin 1, Halley, and Encke have been studied in this way (see Jewitt and Meech 1988, hereafter referred to as JM88) for a summary of the CCD observations and of published infrared observations of a subset of these nuclei. Complementary *in situ* spacecraft measurements of the nucleus of P/Halley (e.g., Keller *et al.* 1987), and radar detections of the nuclei of comets Encke (Kamoun *et al.* 1982) and *IRAS*–Araki–Alcock (Goldstein, Jurgens, and Sekanina 1984) are also available.

The various ground-based observations are valuable since they provide the only data from which the physical properties of a statistical sample of cometary nuclei may be established (spacecraft investigations promise to reveal detailed information on, at most, one or two additional nuclei in the foreseeable future). Optical observations of the above four nuclei, plus radar observations of the nucleus of Comet *IRAS*–Araki–Alcock, suggest a systematic difference between the physical properties of cometary nuclei and main-belt asteroids (JM88). Specifically, the nuclei appear to be highly aspherical in shape compared to main-belt asteroids of comparable size. The difference in shape is intriguing, not least because it is a likely indicator of the different collisional histories experienced by the nuclei and the asteroids. The highly aspherical nuclei might be collisionally unevolved remnants from the formation of the solar system, whereas the asteroids have almost certainly experienced collisional modification of their body shapes. Thus, the comet nucleus observations indicate that the shapes of small solar system bodies are environment dependent. Unfortunately, the number of cometary nuclei for which reliable observations exist is very small, so that any conclusions reached about the statistical properties of nuclei must be regarded with extreme caution. New observations of even a single cometary nucleus are of considerable scientific interest, since they substantially increase the size of the body of knowledge concerning these objects.

Concurrent with the new observations of cometary nuclei, there is a growing awareness that the properties of the cometary coma and those of the nucleus must be intimately related. In large part, this awareness can be traced to high-resolution spacecraft studies of the inner coma of P/Halley, which clearly show collimated coma jets emanating from localized active zones on the irregular nucleus (Keller *et al.* 1987). Cyclic variations in the strength of the coma of that comet (Millis and Sleicher 1986) appear to be related to the rotation of the nucleus, although the physical details of the relationship are presently unclear.

Comet P/Tempel 2 was the subject of a ground-based observational campaign in 1979 (Spinrad, Stauffer, and Newburn 1979; Barker, Cochran, and Rybski 1981; Johnson, Smith, and Shorthill 1981; Tedesco and Barker 1981). The purpose of the present paper is to describe new photometric and spectrophotometric observations of comet P/Tempel 2 (1987g) obtained over a range of heliocentric distances from near aphelion ($Q = 4$ AU) to near perihelion ($q = 1.4$ AU). The observations constitute a uniform and rather detailed dataset from which several of the physical properties of P/Tempel 2 may be deduced. This paper contains our first analyses of the new data.

The new observations were taken to provide answers to the following questions;

What is the rotation state and shape of the nucleus of Tempel 2 and how do the physical properties of this nucleus compare with those of other nuclei?

What are the optical properties of the nucleus (i.e., reflectivity versus wavelength), and how do these properties differ from the optical properties of the coma dust?

At what heliocentric distance does measurable mass loss begin in Tempel 2, and what fraction of the surface participates in the mass loss?

What are the characteristics of the coma, and are these characteristics influenced by the rotation of the nucleus? In

[a] Observations taken at McGraw–Hill Observatory, operated by a consortium consisting of University of Michigan, Dartmouth College, and MIT.

 0004-6256/89/061766-25$00.90

particular, does the rotation force a diurnal variation in the mass loss and, if so, is this variation observable as a travelling wave in the coma surface-brightness profile?

We present, in full, all of the photometry used in the present study, since this will allow independent investigators to use our measurements for their own purposes, should they so choose.

II. OBSERVATIONS

a) CCD Photometry

CCD photometry of P/Tempel 2 was obtained at the McGraw–Hill Observatory on Kitt Peak in Arizona. The 1.3 and 2.4 m telescopes were both operated with CCD cameras placed at the Cassegrainian foci. In addition to their identical $f/7.5$ focal ratios, these telescopes share a number of operational similarities. Both telescopes are guided using the "MIS," intensified CCD finder/guider boxes developed by Matt Johns. The MIS guiders are controlled remotely via Sun computers, which also are used to control the telescope pointing and a majority of the CCD functions. Identical V, R, and I "Mould" interference filters were used at both telescopes.

Two independent CCD cameras, the "MASCOT" and the "BRICC," were employed for the present observations. The MASCOT houses a set of reimaging optics which reduce the effective focal ratios of the telescopes from $f/7.5$ to $f/2.7$, yielding an image scale $s = 0.62''$ per 22 μm pixel on the 2.4 m. The MASCOT chip is 390×594 pixels, with a readout noise of 10 electrons. The BRICC has no-reimaging optics; the image scale at the $f/7.5$ focus of the 1.3 m is $0.48''$ per 22.3 μm pixel. BRICC ACIS CCD is 750×850 pixels and has a 25 electrons readout noise. As well as their low readout noise, the MASCOT and BRICC CCDs are characterized by high linearity and negligible dark emission. Peripheral regions of the CCD were not read out or recorded onto magnetic disk. This "partial readout" reduced the quantity of data recorded to the minimum needed for photometry of the comet and reference field stars, and served to speed all subsequent stages of the data reduction. The Sun computer used to control the readout of the CCD also allowed initial processing of the images to be performed at the telescope. A journal of observations is provided in Table I.

The CCD images were calibrated using bias (zero exposure) frames recorded at intervals throughout each night, plus flatfield frames taken on the morning twilight sky. The "flattened" images were found to be uniform in sensitivity at the $\pm$ 0.5% level across the full width of the chip, with photon-noise-limited flattening at all smaller scales. Errors in the sensitivity calibration among the pixels in the chip contribute negligibly to the final photometric uncertainties, and so are not further discussed. Flux calibration of the images was obtained using standard stars from the lists by Christian *et al.* (1985). The nightly extinction was determined from simultaneous photometry of stars in the Tempel 2 CCD fields. The photometric uncertainties in the comet photometry are primarily due to sky-subtraction uncertainties and zero-point errors. Generally, except for measurements of the outer coma in 1988 June, the photometry is accurate to 0.03–0.05 mag. In the outer coma data, the very low surface brightness (24–25 mag/(arcsec)^2) renders the photometry less certain. A majority of the photometric data were acquired through the R filter, partly because the effective wavelength of this filter ($\lambda_e \approx 6500$ Å) is close to the wavelength of peak quantum efficiency of the CCD, but also because atmospheric extinction and cometary gaseous emissions are less important in the R band than in the more commonly used V band. A few $V - R$ colors were also measured.

TABLE I. Journal of P/Tempel 2 observations.

UT Date	Telescope Diameter [m]	Instrument	Angular Scale ["/pixel]	Work
1987/03/31 - 04/03	KPNO 2.1m	TI 2	0.38	Photometry[1]
1988/02/25, 27 - 29	MHO 2.4 m	MASCOT	0.63	Photometry
1988/04/09, 10, 12, 15	MHO 1.3 m	MASCOT	2.10	Photometry
1988/06/22, 23	MHO 2.4 m	BRICC	0.26	Photometry
1988/06/30 - 07/01	MHO 1.3 m	BRICC	0.48	Photometry
1988/06/26	MHO 2.4 m	Mk III	0.74	Spectra
1988/07/13	KPNO 0.9 m	RCA	0.48	Photometry
1988/09/09	MHO 2.4 m	Mk III	0.74	Spectra

1 See JM88 for complete discussion of these data

We adopt the following notation convention for the photometry of P/Tempel 2. When the comet is demonstrably stellar in appearance (as judged from its surface-brightness profile), the magnitude is simply written m_R, where the "R" denotes the filter used. The stellar magnitudes were generally obtained using a synthetic circular aperture 3″ in radius with sky subtraction from a 3″–5″ radius concentric annulus. These apertures are not critical to the physical interpretation of the photometry, since by definition the stellar magnitudes do not strongly depend on the particular apertures used. When the comet appeared resolved, we employed a set of concentric circular apertures, all centered on the optocenter of P/Tempel 2. The red magnitude integrated within a circular diaphragm of radius p (″) is written $m_R(p'')$. Seven diaphragms of projected angular radii $p = 2.50''$, $3.75''$, $5.00''$, $7.50''$, $10.00''$, $15.00''$ and $20.00''$ were used in this work. The background sky was always determined within a concentric annulus of inner and outer radii $20.00''$ and $30.00''$, respectively, this annulus being essentially devoid of a measurable coma. Occasionally, it is useful to refer to the magnitude within an annulus defined by any two of the circular diaphragms. In such a case, we explicitly list the inner p_i and outer p_o annulus radii as in $m_R(p_i'' - p_o'')$. Thus, for example, $m_R(10'')$ is the magnitude integrated within a circular diaphragm 10″ in radius, while $m_R(5''–10'')$ is the magnitude of the annulus having inner and outer radii 5″ and 10″, respectively.

The geometric circumstances of observation are listed in Table II and shown graphically in Fig. 1. The heliocentric distance R, geocentric distance Δ, and phase angle α, may be determined for any observation mentioned in this paper by reference either to Table II or Fig. 1.

b) CCD Spectra

Spectra of Tempel 2 were obtained using the "Mk III" CCD spectrometer attached to the 2.4 m telescope at McGraw–Hill Observatory. The Mk III utilizes a Thompson 400×576 pixel CCD, cooled to -112 °C by liquid ni-

TABLE II. Geometric parameters.

UT Date	R	Δ	α	Scale [km/"]
1987/03/31 - 04/03	3.99	3.16	9.0	2300
1988/02/25, 27 - 29	2.37	1.95	24.1	1420
1988/04/09, 10, 12, 15	2.09	1.24	19.4	900
1988/06/22 - 23	1.65	0.77	26.0	560
1988/06/30 - 07/01	1.63	0.77	28.0	560
1988/06/26	1.63	0.77	27.7	560
1988/07/13	1.55	0.78	35.2	570
1988/09/09	1.39	0.92	46.6	670

trogen. The read noise is 7 electrons. Dispersion in the Mk III is provided by a set of interchangeable grisms. The observations discussed here were taken using a 300 lines/mm grism blazed at wavelength $\lambda = 5000$ Å and used in the first order. The projected dimensions of the spectrograph slit were $2.8'' \times 320''$. The dimensions of a single 22 μm pixel in the CCD corresponded to 5.1 Å in the dispersion direction and 0.73" in the spatial direction. Projected orientation of the slit on the sky was north–south. The wavelength range of the spectra was determined primarily by the limited blue response of the Mk III reimaging optics; attempted measurements of radiation with $\lambda \leqslant 4400$ Å proved unrewarding. Therefore, the Tempel 2 spectra are restricted to the wavelength range $4400 \leqslant \lambda \leqslant 7200$ Å.

Once again, the MIS, directed to observe the sky reflected in the spectrometer slit plate, served as both finder and guider. The guiding errors on Tempel 2 are estimated at $\pm 0.5''$ (i.e., small compared to the width of the slit). Wavelength calibration of the spectra was obtained using observations of helium–neon and mercury lamps within the MIS. Flux calibration of the spectra was obtained using observations of standard stars from Oke (1974) and Stone (1977). The spectra of different standard stars measured at a range of airmasses were consistent in flux density to $\pm 10\%$ at a given wavelength. This scatter, attributed mainly to slit losses caused by variable atmospheric seeing and to small centering errors, provides a reasonable estimate of the absolute-flux-calibration uncertainty in the Tempel 2 spectra.

Spectra of Tempel 2 in 1988 September were necessarily taken at a larger than optimum airmass. Normally, the airmass is kept as small as possible to minimize atmospheric dispersion, which can cause substantial end-to-end flux-calibration errors in a slit spectrum. For two reasons, we believe that the atmospheric-dispersion errors in our data are small. First, the spectra do not sample the short wavelengths, where atmospheric refraction is largest. Second, we used a wide slit specifically to minimize errors due to differential refraction. Empirically, comparison of spectra taken at large and small airmasses shows no evidence for end-to-end flux errors larger than $\pm 5\%$, corresponding to gradient errors $\leqslant \pm 2\%/1000$ Å.

III. THE PHOTOMETRY

a) 1987 April (R = 4.0 AU)

For reasons of continuity, we include in this paper observations of P/Tempel 2 taken at the Kitt Peak 2.1 m telescope in 1987 April. This photometry, presented first in JM88, is shown for reference in Fig. 2. The photometry shows evidence for nonrandom variations with a range $\Delta m_R \approx 0.3$ mag. No unique period could be found in the P/Tempel 2 light curve; however, the two most significant periods were identified in JM88 as $P = 8.9 \pm 0.1$ and $P = 7.5 \pm 0.1$ hr. As we shall discuss in Sec. IV, the former period is the one that, with the benefit of hindsight, is now identified with the nucleus rotation period.

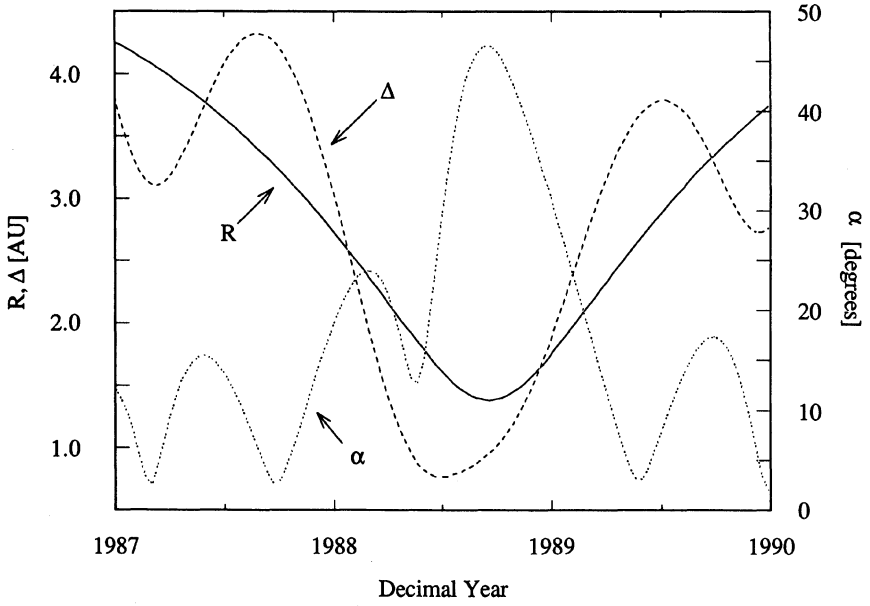

FIG. 1. Geometric circumstances of comet P/Tempel 2 versus date. The figure may be used to estimate the heliocentric distance (R), geocentric distance (Δ), or phase angle (α) for the date of any observation described in this paper.

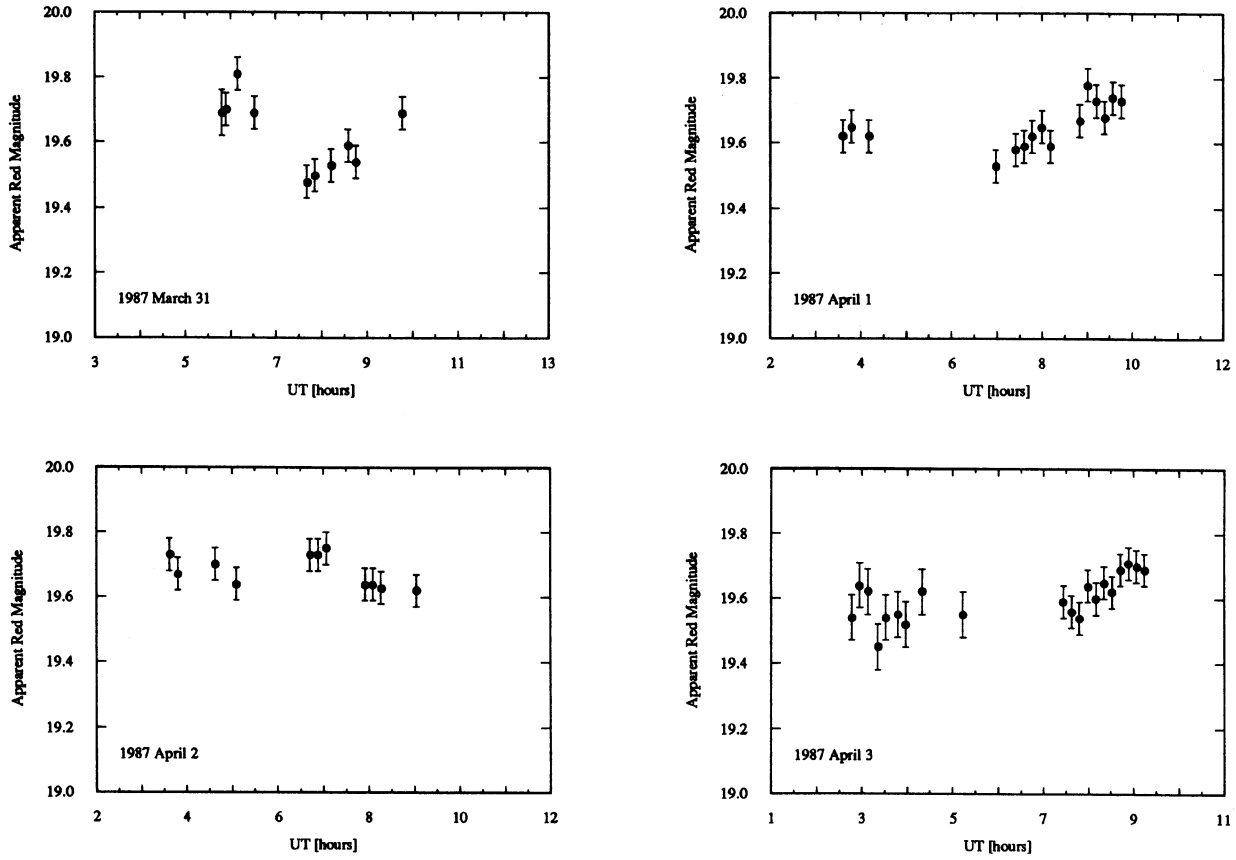

FIG. 2. R filter photometry of P/Tempel 2 from four nights in 1987 April ($R = 3.99$ AU). The integrated magnitude is plotted against the Universal Time of observation. These data are replotted from JM88 to enable direct comparison with the new photometry shown in the accompanying figures.

b) 1988 February ($R = 2.4$ AU)

The comet appeared on the CCD as a stellar object with mean magnitude near $m_R = 18$. A typical CCD image of the comet at this time is shown in Fig. 3 [Plate 104]. We present the integrated photometry in full in Table III, and plot it in Fig. 4. The accuracy of the photometry is determined by uncertainties in the brightness of the night sky (due to faint field stars and galaxies). Figure 4 shows clear evidence for the presence of cyclic variations in the total light. The variations have range $\Delta m \approx 0.65 \pm 0.05$ mag, substantially larger than seen in 1987 April.

c) 1988 April ($R = 2.1$ AU)

By 1988 April the mean magnitude had risen to $m_R \approx 17$, but the comet still appeared stellar at the spatial resolution imposed by the (rather coarse) image scale (2″ per pixel) used in this observing run. The photometry is listed in Table III, and plotted in Fig. 5. The cyclic variations seen in 1988 February persist in 1988 April (Jewitt and Luu 1988) and, again, the light curve has range $\Delta m \approx 0.65 \pm 0.05$ mag. A secular trend toward smaller magnitudes is apparent in the four panels of Fig. 5. This trend is partly an artifact of the observing geometry, which changes substantially over the 6 day observing interval (see Fig. 1), but may also include small contributions from an early, unresolved coma.

d) 1988 June–July ($R = 1.6$–1.5 AU)

A profound morphological change occurred in P/Tempel 2 between 1988 April and 1988 June ($1.6 \leqslant R \leqslant 2.1$ AU), as may be seen by comparing Figs. 3 and 6 [Plate 105]. Tempel 2 was clearly active in 1988 June, as evidenced by an extended and highly asymmetric coma. Figures 6 and 7 show an asymmetric dust coma of radial extent $\rho \approx 20''$ (16 000 km at the comet). The coma shows neither circular nor axial symmetry; the direction of the emission is broadly in position angle 270°, but the image (Fig. 6) also shows an extension along position angle $\sim 150°$ at low surface brightness (extension to the lower right in Fig. 7). Spectra of the comet at this time prove that essentially all (99%) of the light in the R filter passband was sunlight scattered by dust, rather than by molecules. The asymmetry of the coma indicates preferential ejection of dust in the sunward direction.

Integrated photometry from the seven circular apertures (Sec. II*a*) is listed in Table IV and plotted in Fig. 8. Error bars are omitted from Fig. 8 for clarity. The sky was, in all cases, determined from an annulus having projected inner and outer radii 20.0″ and 30.0″, respectively. The figure shows clear variability in the integrated light from each aperture, with the amplitude of variability decreasing markedly with increasing aperture diameter. The strength of the coma may be judged from the observation that $m_R(20.0'') - m_R(2.5'') \approx 1$ mag.

TABLE III. Integrated photometry of comet P/Tempel 2.

N	UT Date	UT	m_R	±	σ_{m_R}	$m_R(1,1,0)$
1	1988 Feb 25	10.417	18.32	±	0.05	13.98
2	1988 Feb 25	10.512	18.32	±	0.05	13.98
3	1988 Feb 25	10.577	18.34	±	0.05	14.00
4	1988 Feb 25	10.642	18.34	±	0.05	14.00
5	1988 Feb 25	10.708	18.36	±	0.05	14.02
6	1988 Feb 25	10.774	18.41	±	0.05	14.07
7	1988 Feb 25	10.839	18.39	±	0.05	14.05
8	1988 Feb 25	10.909	18.48	±	0.05	14.14
9	1988 Feb 25	10.978	18.44	±	0.05	14.10
10	1988 Feb 25	11.046	18.50	±	0.05	14.16
11	1988 Feb 25	11.116	18.59	±	0.05	14.25
12	1988 Feb 25	11.185	18.62	±	0.05	14.28
13	1988 Feb 25	11.251	18.60	±	0.05	14.26
14	1988 Feb 25	11.337	18.69	±	0.05	14.35
15	1988 Feb 25	11.402	18.74	±	0.05	14.40
16	1988 Feb 25	11.470	18.79	±	0.05	14.45
17	1988 Feb 25	11.548	18.79	±	0.05	14.45
18	1988 Feb 25	11.622	18.81	±	0.05	14.47
19	1988 Feb 25	11.693	18.83	±	0.05	14.49
20	1988 Feb 25	11.757	18.88	±	0.05	14.54
21	1988 Feb 25	11.823	18.89	±	0.05	14.55
22	1988 Feb 25	12.023	18.91	±	0.05	14.57
23	1988 Feb 25	12.097	18.91	±	0.05	14.57
24	1988 Feb 25	12.162	18.90	±	0.05	14.56
25	1988 Feb 27	10.812	18.39	±	0.05	14.10
26	1988 Feb 27	10.920	18.32	±	0.05	14.03
27	1988 Feb 27	11.012	18.35	±	0.05	14.06
28	1988 Feb 27	11.107	18.36	±	0.05	14.07
29	1988 Feb 27	11.202	18.33	±	0.05	14.04
30	1988 Feb 27	11.315	18.39	±	0.05	14.10
31	1988 Feb 27	11.426	18.30	±	0.05	14.01
32	1988 Feb 27	11.520	18.36	±	0.05	14.07
33	1988 Feb 27	11.614	18.33	±	0.05	14.04

TABLE III. (continued)

N	UT Date	UT	m_R	±	σ_{m_R}	$m_R(1,1,0)$
34	1988 Feb 27	11.708	18.39	±	0.05	14.10
35	1988 Feb 27	11.805	18.41	±	0.05	14.12
36	1988 Feb 27	11.918	18.47	±	0.05	14.18
37	1988 Feb 27	12.012	18.43	±	0.05	14.14
38	1988 Feb 27	12.107	18.47	±	0.05	14.18
39	1988 Feb 27	12.201	18.56	±	0.05	14.27
40	1988 Feb 27	12.297	18.56	±	0.05	14.27
41	1988 Feb 27	12.390	18.60	±	0.05	14.31
42	1988 Feb 27	12.487	18.58	±	0.05	14.29
43	1988 Feb 27	12.581	18.68	±	0.05	14.39
44	1988 Feb 27	12.674	18.66	±	0.05	14.37
45	1988 Feb 28	9.521	18.28	±	0.05	14.01
46	1988 Feb 28	9.614	18.19	±	0.05	13.92
47	1988 Feb 28	9.708	18.25	±	0.05	13.98
48	1988 Feb 28	9.833	18.34	±	0.05	14.07
49	1988 Feb 28	9.933	18.27	±	0.05	14.00
50	1988 Feb 28	10.027	18.30	±	0.05	14.03
51	1988 Feb 28	10.126	18.29	±	0.05	14.02
52	1988 Feb 28	10.221	18.28	±	0.05	14.01
53	1988 Feb 28	10.318	18.35	±	0.05	14.08
54	1988 Feb 28	10.411	18.41	±	0.05	14.14
55	1988 Feb 28	10.504	18.48	±	0.05	14.21
56	1988 Feb 28	10.599	18.52	±	0.05	14.25
57	1988 Feb 28	10.702	18.67	±	0.05	14.40
58	1988 Feb 28	10.800	18.63	±	0.05	14.36
59	1988 Feb 28	10.897	18.69	±	0.05	14.42
60	1988 Feb 28	11.001	18.72	±	0.05	14.45
61	1988 Feb 28	11.097	18.78	±	0.05	14.51
62	1988 Feb 28	11.193	18.74	±	0.05	14.47
63	1988 Feb 28	11.39	18.88	±	0.05	14.61
64	1988 Feb 28	11.488	18.93	±	0.05	14.66
65	1988 Feb 28	11.587	18.89	±	0.05	14.62
66	1988 Feb 28	11.686	18.81	±	0.05	14.54

TABLE III. (continued)

N	UT Date	UT	m_R	±	σ_{m_R}	$m_R(1,1,0)$
67	1988 Feb 28	11.802	18.88	±	0.05	14.61
68	1988 Feb 28	11.903	18.85	±	0.05	14.58
69	1988 Feb 28	12.005	18.74	±	0.05	14.47
70	1988 Feb 28	12.121	18.75	±	0.05	14.48
71	1988 Feb 29	9.596	18.83	±	0.05	14.58
72	1988 Feb 29	10.658	18.63	±	0.05	14.38
73	1988 Feb 29	10.755	18.62	±	0.05	14.37
74	1988 Feb 29	10.853	18.57	±	0.05	14.32
75	1988 Feb 29	10.948	18.57	±	0.05	14.32
76	1988 Feb 29	11.049	18.49	±	0.05	14.24
77	1988 Feb 29	11.142	18.54	±	0.05	14.29
78	1988 Feb 29	11.258	18.44	±	0.05	14.19
79	1988 Feb 29	11.352	18.42	±	0.05	14.17
80	1988 Feb 29	11.454	18.35	±	0.05	14.10
81	1988 Feb 29	11.550	18.35	±	0.05	14.10
82	1988 Feb 29	11.651	18.26	±	0.05	14.01
83	1988 Feb 29	11.747	18.26	±	0.05	14.01
84	1988 Feb 29	11.844	18.24	±	0.05	13.99
85	1988 Feb 29	11.936	18.21	±	0.05	13.96
86	1988 Feb 29	12.031	18.21	±	0.05	13.96
87	1988 Feb 29	12.124	18.22	±	0.05	13.96
88	1988 Feb 29	12.218	18.23	±	0.05	13.98
89	1988 Feb 29	12.311	18.20	±	0.05	13.95
90	1988 Feb 29	12.404	18.22	±	0.05	13.97
91	1988 Feb 29	12.497	18.28	±	0.05	14.03
92	1988 Feb 29	12.590	18.21	±	0.05	13.96
93	1988 Feb 29	12.684	18.25	±	0.05	14.00
94	1988 April 09	10.395	17.21	±	0.03	14.25
95	1988 April 09	10.509	17.17	±	0.03	14.21
96	1988 April 09	10.618	17.14	±	0.03	14.18
97	1988 April 09	10.724	17.07	±	0.03	14.11
98	1988 April 09	10.828	17.05	±	0.03	14.09
99	1988 April 09	10.934	17.07	±	0.03	14.11

TABLE III. (continued)

N	UT Date	UT	m_R	±	σ_{m_R}	$m_R(1,1,0)$
100	1988 April 09	11.039	16.92	±	0.03	13.96
101	1988 April 09	11.144	16.86	±	0.03	13.90
102	1988 April 09	11.253	16.88	±	0.03	13.92
103	1988 April 09	11.361	16.84	±	0.03	13.88
104	1988 April 09	11.469	16.79	±	0.03	13.83
105	1988 April 10	6.450	16.83	±	0.07	13.91
106	1988 April 10	6.550	16.80	±	0.07	13.88
107	1988 April 10	6.724	16.89	±	0.07	13.97
108	1988 April 10	8.225	17.26	±	0.07	14.34
109	1988 April 10	8.323	17.33	±	0.07	14.41
110	1988 April 10	8.420	17.41	±	0.07	14.49
111	1988 April 10	8.526	17.55	±	0.07	14.63
112	1988 April 10	8.623	17.47	±	0.07	14.55
113	1988 April 10	8.723	17.51	±	0.07	14.59
114	1988 April 10	8.823	17.39	±	0.07	14.47
115	1988 April 10	8.920	17.45	±	0.07	14.53
116	1988 April 10	9.020	17.30	±	0.07	14.38
117	1988 April 10	9.117	17.19	±	0.07	14.27
118	1988 April 10	9.214	17.19	±	0.07	14.27
119	1988 April 10	9.317	17.14	±	0.07	14.22
120	1988 April 10	9.413	17.13	±	0.07	14.21
121	1988 April 10	9.509	17.16	±	0.07	14.24
122	1988 April 10	9.606	17.11	±	0.07	14.19
123	1988 April 10	9.704	17.04	±	0.07	14.12
124	1988 April 10	9.801	16.97	±	0.07	14.05
125	1988 April 10	9.897	16.97	±	0.07	14.05
126	1988 April 10	9.995	17.00	±	0.07	14.08
127	1988 April 10	10.091	16.82	±	0.07	13.90
128	1988 April 10	10.192	16.83	±	0.07	13.91
129	1988 April 10	10.288	16.92	±	0.07	14.00
130	1988 April 10	10.386	16.84	±	0.07	13.92
131	1988 April 10	10.482	16.78	±	0.07	13.86
132	1988 April 10	10.825	16.75	±	0.07	13.83

TABLE III. (continued)

N	UT Date	UT	m_R	±	σ_{m_R}	$m_R(1,1,0)$
133	1988 April 10	10.926	16.74	±	0.07	13.82
134	1988 April 10	11.021	16.77	±	0.07	13.85
135	1988 April 10	11.123	16.81	±	0.07	13.89
136	1988 April 10	11.223	16.90	±	0.07	13.98
137	1988 April 10	11.319	16.88	±	0.07	13.96
138	1988 April 10	11.416	16.94	±	0.07	14.02
139	1988 April 10	11.512	16.97	±	0.07	14.05
140	1988 April 10	11.609	17.01	±	0.07	14.09
141	1988 April 12	10.248	16.96	±	0.03	14.12
142	1988 April 12	10.378	16.91	±	0.03	14.07
143	1988 April 12	10.527	16.85	±	0.03	14.01
144	1988 April 12	10.627	16.83	±	0.03	13.99
145	1988 April 12	10.718	16.79	±	0.03	13.95
146	1988 April 12	11.230	16.69	±	0.03	13.85
147	1988 April 12	11.320	16.69	±	0.03	13.85
148	1988 April 15	6.374	16.55	±	0.02	13.82
149	1988 April 15	6.527	16.56	±	0.02	13.83
150	1988 April 15	6.624	16.50	±	0.02	13.77
151	1988 April 15	6.752	16.45	±	0.02	13.72
152	1988 April 15	6.851	16.45	±	0.02	13.72
153	1988 April 15	6.944	16.40	±	0.02	13.67
154	1988 April 15	7.994	16.76	±	0.02	14.03
155	1988 April 15	8.100	16.79	±	0.02	14.06
156	1988 April 15	8.203	16.91	±	0.02	14.18
157	1988 April 15	8.294	16.86	±	0.02	14.13
158	1988 April 15	8.385	16.90	±	0.02	14.17
159	1988 April 15	8.481	16.93	±	0.02	14.20
160	1988 April 15	8.574	17.01	±	0.02	14.28
161	1988 April 15	8.770	17.03	±	0.02	14.30
162	1988 April 15	8.888	17.04	±	0.02	14.31
163	1988 April 15	9.114	17.02	±	0.02	14.29
164	1988 April 15	9.372	17.00	±	0.02	14.27
165	1988 April 15	9.497	16.94	±	0.02	14.21

TABLE III. (continued)

N	UT Date	UT	m_R	±	σ_{m_R}	$m_R(1,1,0)$
166	1988 April 15	9.683	16.89	±	0.02	14.16
167	1988 April 15	9.778	16.87	±	0.02	14.14
168	1988 April 15	9.869	16.85	±	0.02	14.12
169	1988 April 15	9.962	16.79	±	0.02	14.06
170	1988 April 15	10.056	16.76	±	0.02	14.03
171	1988 April 15	10.148	16.72	±	0.02	13.99
172	1988 April 15	10.241	16.70	±	0.02	13.97
173	1988 April 15	10.334	16.61	±	0.02	13.88
174	1988 April 15	10.427	16.63	±	0.02	13.90
175	1988 April 15	10.518	16.62	±	0.02	13.89
176	1988 April 15	10.610	16.59	±	0.02	13.86
177	1988 April 15	10.704	16.60	±	0.02	13.87
178	1988 April 15	10.797	16.60	±	0.02	13.87
179	1988 April 15	10.899	16.49	±	0.02	13.76
180	1988 April 15	11.014	16.52	±	0.02	13.79
181	1988 April 15	11.119	16.50	±	0.02	13.77
182	1988 April 15	11.210	16.51	±	0.02	13.78
183	1988 April 15	11.303	16.49	±	0.02	13.76
184	1988 April 15	11.397	16.52	±	0.02	13.79
185	1988 April 15	11.488	16.47	±	0.02	13.74

IV. THE SPECTRA

a) 1988 June (R = 1.6 AU)

A typical CCD reflectivity spectrum of Tempel 2 is shown in Fig. 9. The reflectivity was computed by dividing the comet spectrum by a spectrum of the solar-analog star 16 Cyg A, and normalizing the ratio to unity at $\lambda = 5800$ Å. The spectrum refers to a 2.8″ × 10.0″ rectangular area centered on the nucleus and with the long axis oriented north–south. The spectrum shows a strong reflection continuum, with a weak, superimposed emission band due to C_2 at $\lambda \approx 5173$ Å and forbidden emission from [O I] at $\lambda \approx 6300$ and 6363 Å. The reflectivity gradient of the continuum in Fig. 9 is $S' \approx 10\% \pm 2\%/1000$ Å. A significant fraction of the light recorded in the spectrum in Fig. 9 is scattered directly from the cometary nucleus. The fractional contribution of the nucleus to the spectrum in Fig. 9 is quantitatively assessed in Sec. V.

b) 1988 September (R = 1.39 AU)

In Fig. 10 we show three reflectivity spectra extracted from a two-dimensional CCD spectrum taken UT 1988 September 9. The reflectivity spectra, which refer to three distinct areas on the coma of Tempel 2, were again computed using observations of the solar analog 16 Cyg A. Spectrum (a) was extracted from a rectangular area centered on the nucleus and with projected dimensions 2.8″ EW × 7.0″ NS. Spectrum (b) was extracted from a rectangle of dimensions 2.8″ EW × 14.0″ NS, centered 10.5″ N of the nucleus. Spectrum (c) was extracted from a 2.8″ EW × 44.1″ NS rectangle centered 40.6″ N of the nucleus. Thus, spectrum (a) includes radiation scattered from the nucleus plus from the near-nucleus coma, while spectra (b) and (c) contain only coma emission.

All three spectra show a rich set of emission bands due to C_2, NH_2, and [O I]. Some of the major bands are indicated in Fig. 10. The ratio of the emission-band flux to the continuum flux clearly increases with increasing distance from the nucleus, as is expected from the known scale lengths of the observed radicals. Perhaps more surprising is the difference in the slope of the reflectivity seen between the central spectrum (a) and the coma spectra ((b) and (c)). Spectrum (a) shows a continuum that is clearly reddened with respect to the solar continuum. The reflectivity gradient is $S' \approx 15\% \pm 2\%/1000$ Å, consistent with the 1988 June gradient (Sec. IV*a*) within the uncertainties of measurement. The continuum in (b) and (c) is more nearly neutral, with $S' \approx 1\% \pm 3\%/1000$ Å. One might be tempted to ascribe the neutrality of the continuum in coma spectra (b) and (c) to molecular contamination of the continuum "windows" at the blue end of the sampled spectra. An argument against

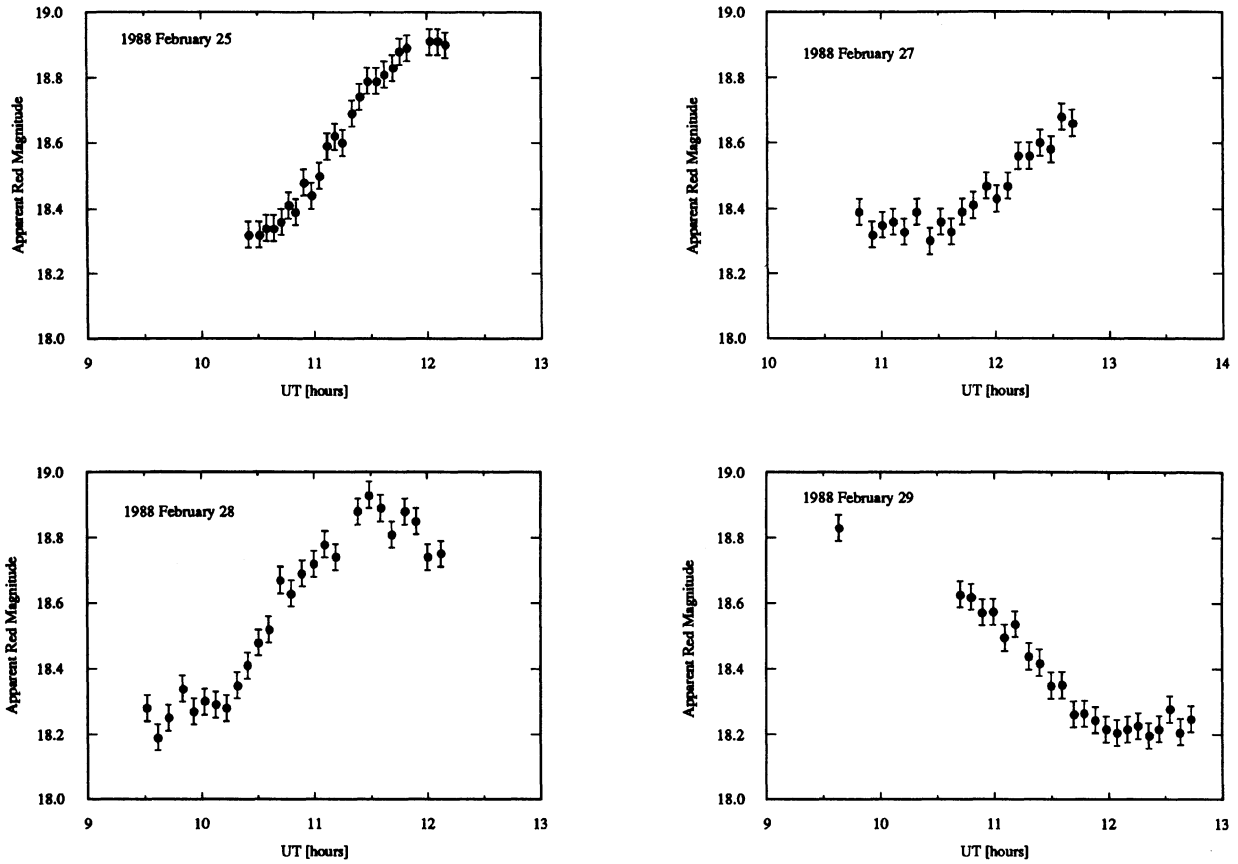

FIG. 4. R filter photometry of P/Tempel 2 from four nights in 1988 February ($R = 2.37$ AU). The integrated magnitude is plotted against the Universal Time of observation.

this possibility is that the two coma spectra, (b) and (c), show identically neutral continua, whereas one would expect the continuum at larger projected distance (spectrum (c)) to appear bluer, in concordance with the increased gas/dust ratio at larger distances. In addition, the linearity of the continua in all three spectra would not be a natural consequence of selective gas contamination at the blue wavelengths. Therefore, we interpret Fig. 10 as evidence for a spatial color variation across the coma of comet P/Tempel 2. As we describe below, the red central continuum is mostly due to the nucleus, while the neutral continuum is attributed to the coma grains.

V. DISCUSSION

a) Nucleus Rotation

To search for periodicities in the photometry, we first correct the apparent magnitudes to absolute magnitudes using

$$m_R(1,1,0) = m_R - 5\log(R\Delta) - \beta\alpha\,. \quad (1)$$

The quantity on the left is the magnitude of the comet as it would appear at unit heliocentric and geocentric distances, and zero degrees phase angle. An empirical phase coefficient $\beta = 0.04$ mag/deg was used. This correction removes variations in the apparent magnitude due to variable observing geometry within each monthly dataset.

A "string length" period search (Dworetsky 1983) applied to the absolute magnitudes from 1988 February reveals several possible periods. The deepest string-length minimum and the most convincing phase plot are produced by the synodic period

$$P_{\mathrm{FEB88}} = 8.94 \pm 0.01 \text{ hr}. \quad (2)$$

The phase plot shows a two-peaked light curve with a slight asymmetry between the peaks (Fig. 11(b)). Our best estimate of the mean absolute magnitude in 1988 February is

$$m_R(1,1,0)_{\mathrm{FEB88}} = 14.3 \pm 0.1, \quad (3)$$

where the quoted uncertainty is mostly due to the uncertain phase coefficient β.

The April photometry was used to obtain an estimate of the rotation period, again using the string-length method applied to absolute magnitudes. The derived period,

$$P_{\mathrm{APR88}} = 8.95 \pm 0.01 \text{ hr}, \quad (4)$$

is completely independent of, but nevertheless equal to, P_{FEB88} within the uncertainties of measurement. Our best estimate of the mean absolute magnitude in 1988 April is

$$m_R(1,1,0)_{\mathrm{APR88}} = 14.3 \pm 0.1. \quad (5)$$

The phase plot computed using Eq. (4) is shown in Fig. 11(c).

The period of variation in 1988 June is more difficult to estimate because of the contaminating effects of a variable coma. In fact, a string search in m_R (2.5″) does show a mini-

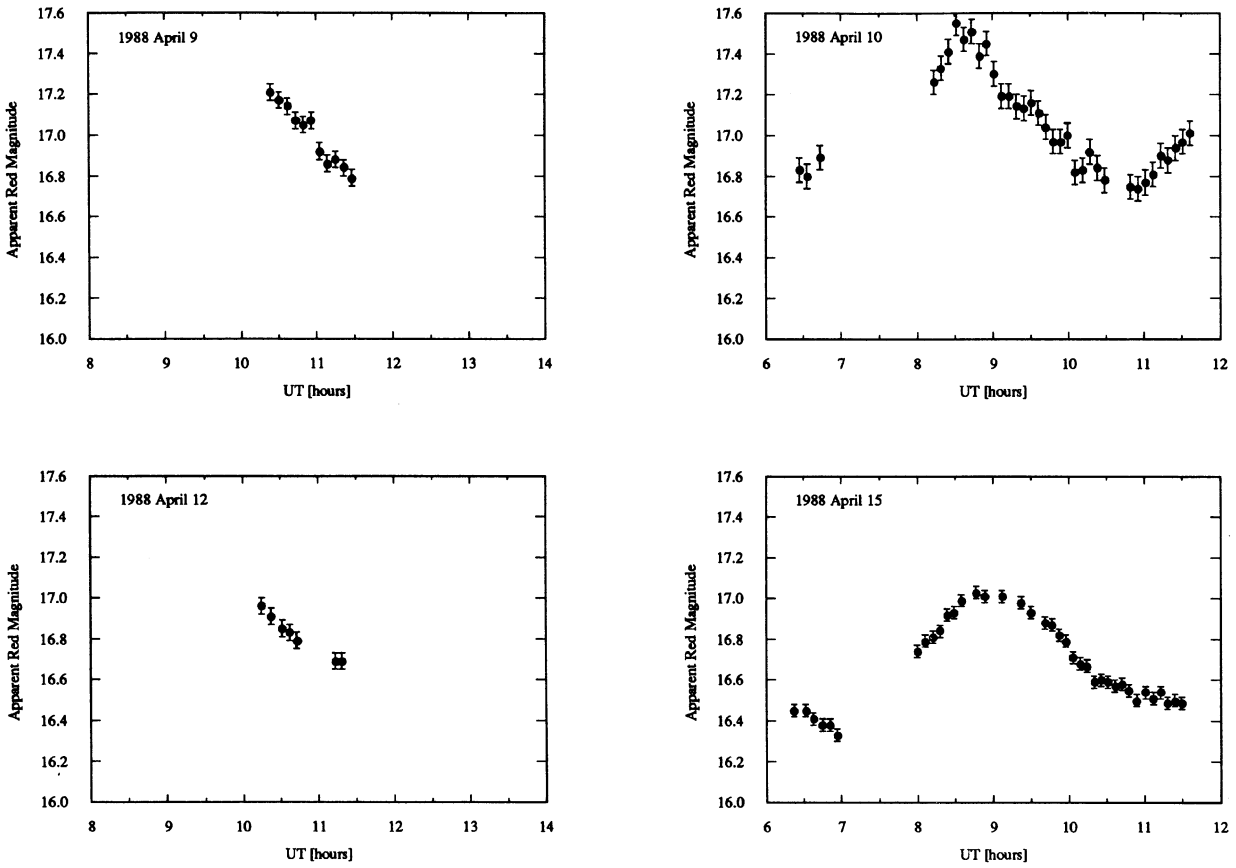

FIG. 5. R filter photometry of P/Tempel 2 from four nights in 1988 April ($R = 2.08$ AU). The integrated magnitude is plotted against the Universal Time of observation.

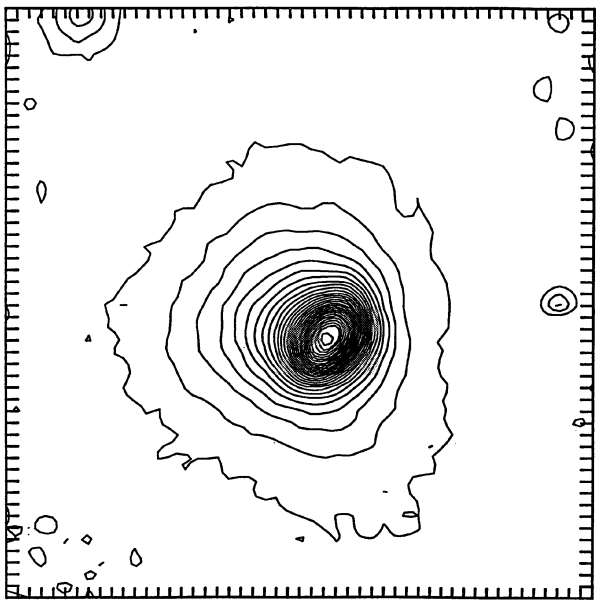

FIG. 7. Contour plot of a section of the image shown in Fig. 6. The difference of the logarithms of the surface brightness measured on adjacent contours equals 0.05. The image was smoothed with a 2×2 pixel rectangular filter prior to computation of the contours. The image section shown has the same orientation as Fig. 6 and is 38″ square.

mum near 9 hr, but with considerable scatter due to the coma. To more reliably estimate the period, we took advantage of the spatial information contained in our June surface photometry (Table IV) to subtract the coma from the central m_R (2.5″) photometry, presumably yielding a better approximation to the true nucleus magnitude. From the string-length method applied to the coma-subtracted nucleus magnitude, we find

$$P_{\mathrm{JUN88}} = 8.97 \pm 0.02 \text{ hr}, \quad (6)$$

where the larger uncertainty is presumably a result of interference in the nucleus light curve by the coma. Within the enlarged uncertainty, the June period is consistent with the periods identified in the February and April data. The mean absolute magnitude of the nucleus in 1988 June is

$$m_R(1,1,0)_{\mathrm{JUN88}} = 14.3 \pm 0.2. \quad (7)$$

A phase plot constructed from the nucleus magnitudes is shown in Fig. 11(d).

For reference, we note that JM88 found possible periods

$$P_{\mathrm{APR87}} = 8.9 \pm 0.1 \quad \text{and} \quad 7.5 \pm 0.1 \text{ hr} \quad (8)$$

and mean absolute magnitude

$$m_R(1,1,0)_{\mathrm{APR87}} = 13.8 \pm 0.1 \quad (9)$$

from independent photometry in 1987 April. The corresponding phase plot from the 8.95 hr period is shown in Fig. 11(a).

TABLE IV. Spatially resolved photometry of comet P/Tempel 2.

N	UT Date	UT Start	m(2.5")	m(3.75")	m(5.0")	m(7.5")	m(10.0")	m(15.0")	m(20.0")
1	1988 June 22	4.2294	15.432	15.102	14.932	14.672	14.502	14.372	14.322
2	1988 June 22	4.3227	15.433	15.093	14.913	14.613	14.483	14.353	14.303
3	1988 June 22	4.4144	15.413	15.083	14.913	14.633	14.483	14.353	14.293
4	1988 June 22	4.5097	15.393	15.073	14.913	14.703	14.503	14.353	14.303
5	1988 June 22	4.6016	15.354	15.054	14.894	14.704	14.584	14.364	14.304
6	1988 June 22	4.6933	15.334	15.034	14.884	14.694	14.574	14.394	14.294
7	1988 June 22	4.7933	15.314	15.024	14.874	14.684	14.574	14.454	14.334
8	1988 June 22	4.8927	15.334	15.024	14.864	14.674	14.554	14.454	14.384
9	1988 June 22	4.9861	15.314	15.014	14.854	14.664	14.544	14.414	14.374
10	1988 June 22	5.0775	15.294	15.004	14.854	14.664	14.544	14.424	14.384
11	1988 June 22	5.1683	15.354	15.034	14.864	14.674	14.554	14.434	14.404
12	1988 June 22	5.2597	15.353	15.023	14.863	14.663	14.543	14.413	14.363
13	1988 June 22	5.3519	15.323	15.023	14.863	14.673	14.553	14.423	14.383
14	1988 June 22	5.4564	15.303	15.013	14.863	14.673	14.553	14.423	14.383
15	1988 June 22	5.5480	15.312	15.022	14.862	14.672	14.542	14.402	14.332
16	1988 June 22	5.6397	15.302	15.022	14.872	14.682	14.562	14.432	14.382
17	1988 June 22	5.7314	15.311	15.031	14.881	14.681	14.561	14.421	14.371
18	1988 June 22	5.8236	15.400	15.070	14.900	14.690	14.570	14.430	14.379
19	1988 June 22	6.0152	15.339	15.069	14.909	14.709	14.589	14.439	14.409
20	1988 June 22	6.1508	15.367	15.087	14.927	14.727	14.597	14.447	14.387
21	1988 June 22	6.2439	15.396	15.116	14.956	14.746	14.616	14.476	14.406
22	1988 June 22	6.3361	15.435	15.135	14.965	14.765	14.625	14.485	14.435
23	1988 June 22	6.4277	15.464	15.164	14.994	14.784	14.664	14.524	14.484
24	1988 June 22	6.5202	15.463	15.172	15.012	14.793	14.663	14.523	14.473
25	1988 June 22	6.6116	15.491	15.201	15.031	14.821	14.691	14.551	14.511
26	1988 June 22	6.7027	15.520	15.220	15.060	14.840	14.700	14.560	14.500
27	1988 June 22	6.7947	15.518	15.238	15.068	14.848	14.708	14.558	14.498
28	1988 June 22	6.8916	15.566	15.266	15.096	14.876	14.746	14.596	14.546
29	1988 June 22	6.9833	15.584	15.284	15.114	14.894	14.764	14.614	14.564
30	1988 June 22	7.0764	15.592	15.302	15.122	14.902	14.762	14.612	14.552

TABLE IV. (continued)

N	UT Date	UT Start	m(2.5")	m(3.75")	m(5.0")	m(7.5")	m(10.0")	m(15.0")	m(20.0")
31	1988 June 22	7.1683	15.600	15.300	15.130	14.910	14.770	14.630	14.580
32	1988 June 22	7.2611	15.628	15.308	15.128	14.898	14.757	14.597	14.528
33	1988 June 22	7.3555	15.615	15.305	15.125	14.895	14.765	14.615	14.565
34	1988 June 22	7.4583	15.602	15.292	15.122	14.902	14.762	14.622	14.572
35	1988 June 22	7.5511	15.589	15.279	15.109	14.889	14.749	14.589	14.529
36	1988 June 22	7.6427	15.636	15.296	15.106	14.886	14.746	14.606	14.546
37	1988 June 22	8.2864	15.427	15.127	14.967	14.767	14.637	14.487	14.357
38	1988 June 22	8.3833	15.401	15.101	14.951	14.751	14.631	14.491	14.381
39	1988 June 23	5.5623	15.680	15.310	15.110	14.870	14.730	14.580	14.530
40	1988 June 23	5.6769	15.660	15.300	15.100	14.860	14.710	14.570	14.520
41	1988 June 23	5.7678	15.630	15.300	15.100	14.870	14.730	14.580	14.530
42	1988 June 23	5.8583	15.650	15.300	15.110	14.880	14.740	14.590	14.530
43	1988 June 23	5.9489	15.610	15.270	15.080	14.850	14.710	14.570	14.520
44	1988 June 23	6.0417	15.590	15.270	15.080	14.850	14.720	14.570	14.520
45	1988 June 23	6.1308	15.560	15.220	15.030	14.800	14.660	14.510	14.440
46	1988 June 23	6.2217	15.530	15.220	15.050	14.820	14.690	14.540	14.490
47	1988 June 23	6.3110	15.540	15.210	15.020	14.800	14.670	14.540	14.490
48	1988 June 23	6.4861	15.500	15.190	15.020	14.800	14.670	14.540	14.480
49	1988 June 23	6.5769	15.460	15.170	15.000	14.790	14.660	14.510	14.450
50	1988 June 23	6.6681	15.450	15.160	14.990	14.780	14.650	14.510	14.450
51	1988 June 23	6.7589	15.430	15.140	14.980	14.770	14.650	14.510	14.470
52	1988 June 23	7.0831	15.380	15.100	14.940	14.740	14.610	14.470	14.410
53	1988 June 23	7.1750	15.350	15.090	14.940	14.750	14.630	14.520	14.480
54	1988 June 23	7.2664	15.360	15.090	14.940	14.750	14.630	14.500	14.460
55	1988 June 23	7.5750	15.360	15.080	14.930	14.730	14.610	14.330	14.250
56	1988 June 30	4.5617	15.142	14.902	14.742	14.552	14.432	14.293	14.222
57	1988 June 30	4.6672	15.162	14.892	14.742	14.543	14.422	14.283	14.242
58	1988 June 30	4.7586	15.120	14.860	14.710	14.510	14.380	14.220	14.140
59	1988 June 30	4.8517	15.110	14.860	14.720	14.520	14.390	14.240	14.170
60	1988 June 30	4.9425	15.120	14.860	14.720	14.530	14.410	14.260	14.200
61	1988 June 30	5.0344	15.127	14.868	14.727	14.538	14.418	14.288	14.238
62	1988 June 30	5.1261	15.105	14.855	14.715	14.525	14.405	14.265	14.195
63	1988 June 30	5.2169	15.105	14.865	14.725	14.535	14.405	14.265	14.215
64	1988 June 30	5.3092	15.103	14.872	14.733	14.533	14.403	14.263	14.203

TABLE IV. (continued)

N	UT Date	UT Start	m(2.5")	m(3.75")	m(5.0")	m(7.5")	m(10.0")	m(15.0")	m(20.0")
65	1988 June 30	5.4036	15.130	14.870	14.720	14.520	14.400	14.260	14.190
66	1988 June 30	5.4953	15.127	14.877	14.738	14.537	14.408	14.258	14.207
67	1988 June 30	5.5894	15.175	14.905	14.755	14.555	14.425	14.285	14.225
68	1988 June 30	5.6811	15.233	14.943	14.782	14.583	14.443	14.312	14.263
69	1988 June 30	5.7725	15.230	14.950	14.790	14.580	14.450	14.300	14.230
70	1988 June 30	5.8658	15.225	14.945	14.785	14.585	14.465	14.315	14.255
71	1988 June 30	5.9864	15.280	14.990	14.830	14.610	14.480	14.330	14.280
72	1988 June 30	6.0825	15.328	14.998	14.828	14.607	14.457	14.307	14.238
73	1988 June 30	6.3836	15.380	15.060	14.880	14.650	14.500	14.330	14.250
74	1988 June 30	6.5111	15.395	15.105	14.925	14.695	14.565	14.425	14.365
75	1988 June 30	6.6031	15.507	15.167	14.978	14.728	14.577	14.417	14.337
76	1988 June 30	6.6978	15.490	15.160	14.960	14.720	14.580	14.410	14.350
77	1988 June 30	6.7889	15.482	15.172	14.982	14.732	14.592	14.443	14.373
78	1988 June 30	6.8797	15.557	15.227	15.038	14.797	14.647	14.497	14.427
79	1988 June 30	6.9700	15.610	15.230	15.020	14.760	14.610	14.450	14.400
80	1988 June 30	7.0611	15.580	15.220	14.960	14.760	14.600	14.420	14.360
81	1988 June 30	7.1536	15.583	15.212	15.013	14.772	14.612	14.452	14.403
82	1988 June 30	7.2458	15.573	15.202	14.993	14.733	14.573	14.403	14.343
83	1988 June 30	7.3367	15.592	15.213	15.002	14.752	14.602	14.443	14.393
84	1988 June 30	7.4278	15.550	15.180	14.990	14.740	14.590	14.440	14.390
85	1988 June 30	7.5186	15.538	15.157	14.958	14.687	14.538	14.378	14.308
86	1988 June 30	7.6092	15.505	15.125	14.925	14.655	14.505	14.315	14.215
87	1988 June 30	7.7000	15.503	15.122	14.913	14.663	14.513	14.343	14.263
88	1988 June 30	7.7914	15.508	15.117	14.918	14.668	14.508	14.338	14.258
89	1988 June 30	7.9100	15.485	15.105	14.905	14.645	14.495	14.345	14.255
90	1988 June 30	8.0164	15.495	15.085	14.885	14.645	14.505	14.355	14.285

The persistence of the $P = 8.95 \pm 0.01$ hr period in P/Tempel 2 photometry obtained in three observing runs spread over 5 months in 1988 (see also Wisniewski 1988), together with a consistent period in photometry from 1987 April, strongly suggests modulation of the scattered light by a rotating, aspherical nucleus. Variations due to activity on the nucleus are hardly likely to yield so constant a period (unless such activity is itself modulated by nucleus rotation). Therefore, we identify $P = 8.95 \pm 0.01$ hr with the synodic period of rotation of the nucleus of comet P/Tempel 2.

This interpretation is strengthened by the long-term photometric behavior of the comet. A plot of the cometary magnitude versus the date of observation is presented in Fig. 12. The vertical bars in the plot delineate the range of intrinsic variability of the comet at each epoch of observation, rather than uncertainties in the photometry (the latter uncertainties are too small to be seen at the scale of the graph). In all but the June–July photometry, we have plotted the integrated light from the comet. In June–July we separately plot the light from the central 2.5" radius photometry aperture, plus the light from a 20" radius aperture. Also shown in the figure is the inverse-square law for a phase-darkened spherical nucleus, given by Eq. (1). Two curves are plotted, one with $m_R(1,1,0) = 14.0$, $\beta = 0.03$ mag/deg and the other with $m_R(1,1,0) = 14.0$, $\beta = 0.04$ mag/deg. It is evident that both models provide reasonable fits to the photometry. We interpret this good fit to support the notion that the photometry refers to the phase-darkened nucleus, and that the influence of any coma in Fig. 12 is small until 1988 June. The inferred large phase coefficient, $\beta = 0.035 \pm 0.005$ mag/deg, is expected for a low-albedo surface, as has been found

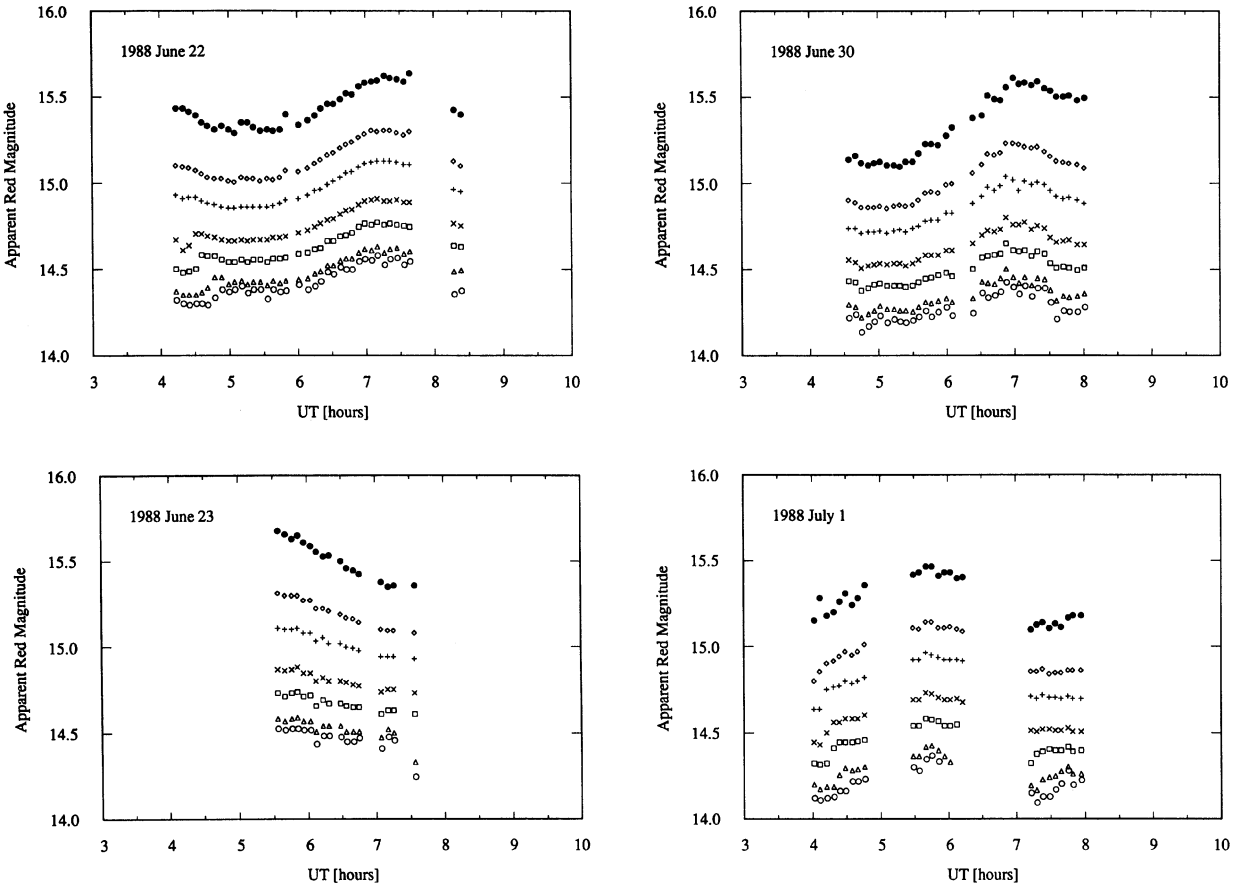

FIG. 8. *R* filter photometry of P/Tempel 2 from four nights in 1988 June ($R \approx 1.63$ AU). The magnitude integrated within each of seven apertures is plotted versus the Universal Time of observation. The angular radii of the apertures, plotted from top to bottom within each figure, are 2.5″, 3.75″, 5.0″, 7.5″, 10.0″, 15.0″, and 20.0″. The sky signal was determined from a concentric annulus with inner and outer radii of 20.0″ and 30.0″, respectively.

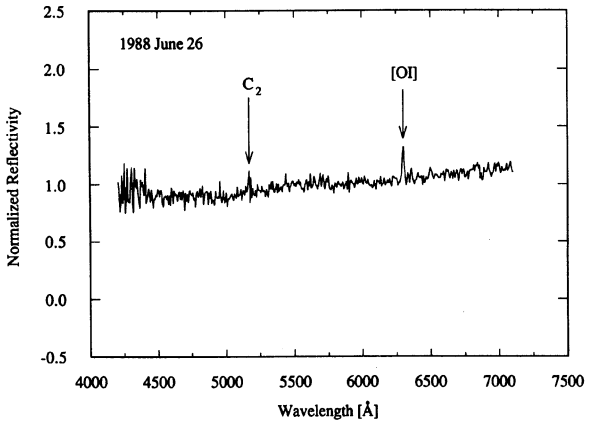

FIG. 9. CCD reflectivity spectrum of P/Tempel 2 taken 1988 June 26 ($R = 1.63$ AU). This is a 1200 s integration using the Mk III spectrograph on the 2.4 m telescope. The extracted spectrum is from a 2.8″ × 7″ rectangle centered on the comet. The figure shows weak gas emission superimposed upon a strong, linear continuum. Increased noise at the blue end of the spectrum is caused by the low quantum efficiency of the CCD at these wavelengths.

from infrared observations by A'Hearn *et al.* (1988a). We note that *exact* agreement between the spherical-asteroid models and the photometry in Fig. 12 is not to be expected (at the ≈ few × 0.1 mag level), even in the complete absence of a coma, since our own photometry shows that the nucleus is aspherical, and thus may not be well represented by the model.

It is possible to combine the photometric data from all three months of detailed observation to derive the sidereal (as opposed to synodic) rotation period of the nucleus. It is also possible to use the secular variations in the photometric range of the light curves to determine the direction of the rotation pole of the nucleus. It seems prudent to delay these exercises in print until a corresponding set of high-quality photometric observations of Tempel 2 has been obtained on the outbound (post-perihelion) leg of the orbit, since these observations will presumably add considerable weight to any conclusions we might reach about the spin pole and the sidereal period based only on the pre-perihelion data. For now, we merely note that the variations in the light-curve range are consistent with the rotation pole predicted by Sekanina (1988a) on the basis of observations of the asymmetric coma of this comet in previous apparitions. We further

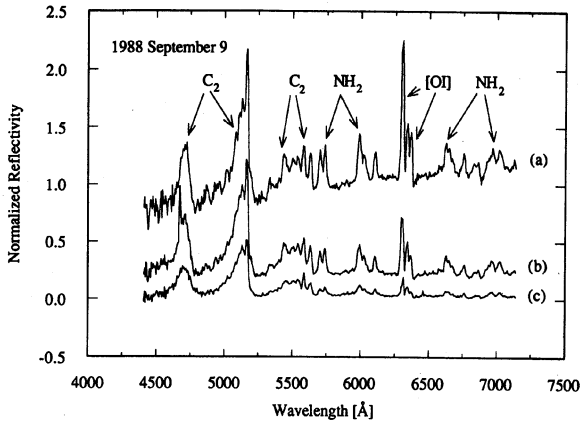

FIG. 10. Reflectivity spectra of three regions on P/Tempel 2 taken UT 1988 September 9 at $3^h\ 13^m$ ($R = 1.39$ AU). All three spectra were extracted from a 300 s image taken using the Mk III spectrograph on the 2.4 m telescope. The mean surface brightness ($Wm^{-2}\ Hz^{-1}\ arcsec^{-2}$) within each region has been divided by the solar spectrum to compute reflectivity. Each spectrum has been further normalized to the reflectivity at $\lambda = 5800$ Å in spectrum (a), so that the correct relative intensities are visible. Spectrum (a) corresponds to a $7.0'' \times 2.8''$ rectangle centered on the nucleus and includes nucleus and coma emission, while spectrum (b) is from a $14.0'' \times 2.8''$ rectangle with center displaced 10.5" N from the nucleus, and (c) is from a $44.1'' \times 2.8''$ rectangle centered 40.6" N of the nucleus. Prominent emission features from the gas coma are identified.

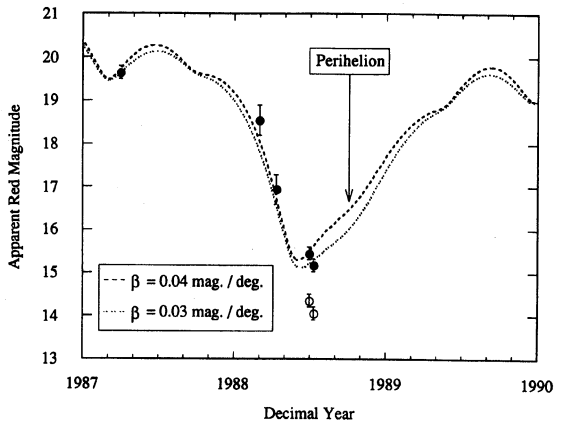

FIG. 12. The mean R magnitude of Tempel 2 is plotted versus the epoch of observation, for the interval encompassing the 1985–1989 perihelion to aphelion leg of the orbit. The vertical bars on the measurements delineate the range of magnitudes measured at the respective epoch (photometry error bars are too small to be discerned at the scale of the graph). Solid dots denote measurements of the nucleus magnitude, while hollow dots denote m_R (20.0"). The two lines show the "asteroidal model" of the nucleus described in the text (see Eq. (1)), with phase coefficients $\beta = 0.04$ mag deg^{-1} and $\beta = 0.03$ mag deg^{-1}, as indicated.

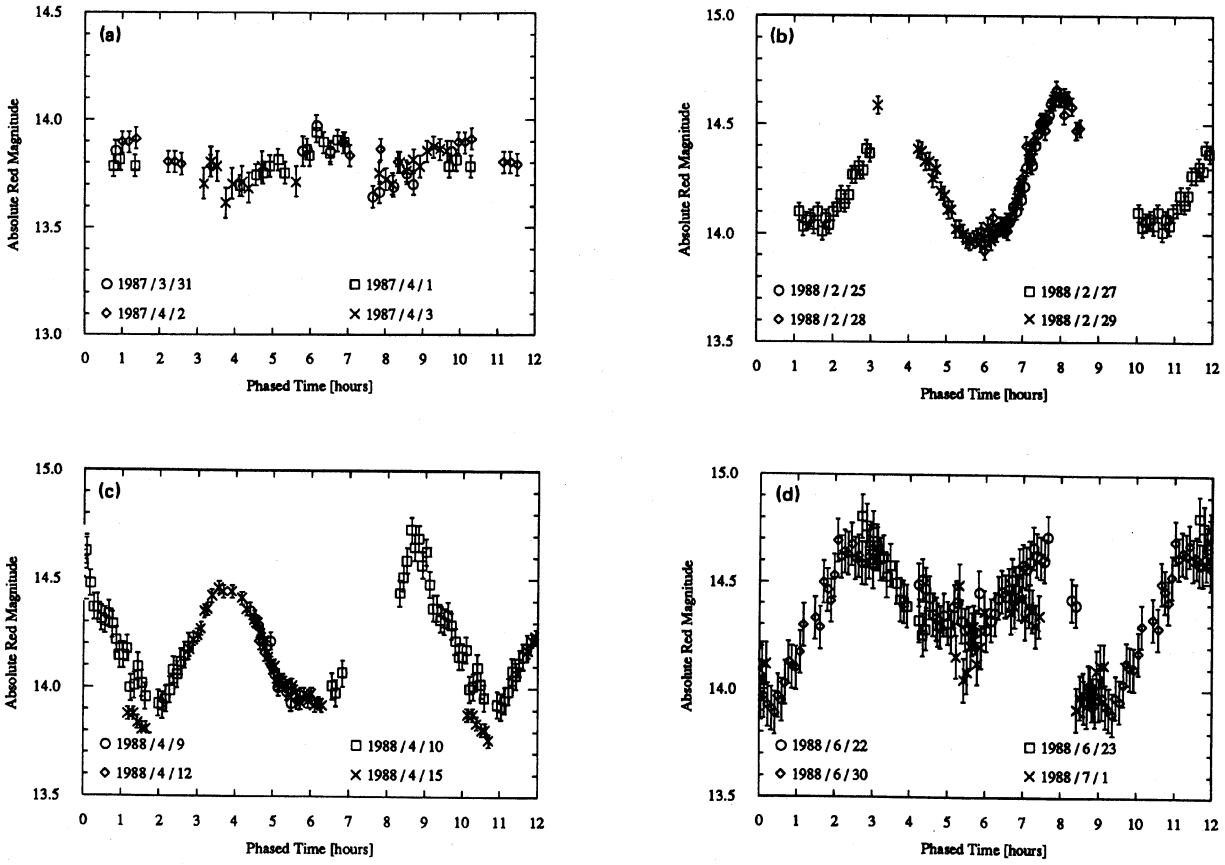

FIG. 11. Phase plots from photometry of P/Tempel 2. The plots correspond to observations from (a) 1987 April, (b) 1988 February, (c) 1988 April, and (d) 1988 June. The larger error bars plotted in (d) are introduced by the correction for coma contamination of the nucleus light.

note that the derived synodic period is inconsistent with the 4.8 hr period estimated by Whipple (1982) from his "halo method."

b) Nucleus Shape

Long-term variations in the absolute magnitude m_R (1,1,0) and photometric range Δm_R of the nucleus may be used to estimate the nucleus shape. These quantities are summarized in Table V (the entry for 1988 June includes a correction for coma contamination of the nucleus magnitude). The most striking observations to be made from the table are that (1) m_R(1,1,0) increased by $\sim$0.5 mag between 1987 April and 1988 February, and has remained constant in all subsequent observations, and (2) that the range increased from $\Delta m_R = 0.3 \pm 0.1$ mag to $\Delta m_R = 0.65 \pm 0.05$ mag between 1987 and 1988. The variations in m_R (1,1,0) are too large to be attributed to observational error, and too large to be due to an error in the phase coefficient. We seek an explanation in terms of the changing projection of the aspherical nucleus on the plane of the sky.

We represent the nucleus by a triaxial body, with axes a and b in the rotational equator and c perpendicular to a and b. The possibility that the nucleus is precessing is not strongly constrained by the present intermittently sampled photometry. It is both simple and illuminating to estimate the a:b and b:c axis ratios by inspection of Fig. 11. The large rotational range in the 1988 photometry suggests that the sub-Earth point was near the cometocentric equator. The minima and maxima in $m_R(1,1,0)_{1988}$, when substituted into the inverse-square law with $R = \Delta = 1$ and $\alpha = 0$, give the equatorial projections ac and bc, respectively. From the $\Delta m_R = 0.7$ mag rotational variation observed in 1988 February, April, and June, we estimate $a{:}b = 10^{0.4\Delta m} = 1.9{:}1$. Formally, this is a lower limit to a:b, since we may not be seeing a true equatorial projection. The reduced Δm_R in 1987 April may suggest that the nucleus was then viewed from a more nearly polar perspective than in 1988, so that $m_R(1,1,0)_{APR87}$ gives an approximation to ab (the polar projection in the plane of the sky). From the equality between the *mean* m_R(1,1,0) in 1987 and the *maximum* light in $m_R(1,1,0)_{1988}$, we infer $ab \approx ac$, so $b \approx c$. Thus the nucleus is prolate spheroidal, with axes $a{:}b{:}c \approx 1.9{:}1{:}1$, and is in rotation around one of the minor axes (c).

We note that the b:c axis ratio is much less certain than the a:b axis ratio, mainly because a totally different interpretation may be assigned to the smaller m_R(1,1,0) in the 1987 data. The $\Delta m \approx 0.5$ mag excess brightness of the absolute magnitude and the reduced photometric range (from 0.70 to 0.35 mag; see Fig. 11 and Table VI) are both consistent with the presence of a coma in 1987 April, with a cross section comparable to the nucleus cross section. The only evidence against this interpretation is from our finding (discussed in Sec. V*h*) that the nucleus and the coma possess different optical colors. The color of P/Tempel 2 in 1987 April was similar to the color of the bare nucleus, not to the color of the coma dust, suggesting that coma contamination was minimal in 1987 April. Therefore, we tentatively proceed on the assumption that the b:c axis ratio is correct, but we keep in mind the possibility that it may not be. Of course, the a:b ratio is unaffected by the uncertainty in b:c.

The nucleus data summarized in Table V may be used to estimate the absolute dimensions of the nucleus once the geometric albedo is known. We use a geometric albedo $p_R = 0.024 \pm 0.005$ (A'Hearn *et al.* 1988a) to find

$$a{:}b{:}c = 8{:}4{:}4 \text{ km}. \quad (10)$$

The dimensions of the nucleus of P/Tempel 2 (see also Sekanina 1988b) are thus similar to those of P/Halley ($8 \times 4 \times 4$ km; Keller *et al.* 1987).

The asphericity of the P/Tempel 2 nucleus is typical of the shapes of all cometary nuclei so far studied with CCDs, while the $\sim$9 hr rotation period is the shortest of those yet determined with confidence. This is clearly apparent in Fig. 13, where we plot the photometric range versus the logarithm of the rotation period for five nuclei for which these quantities are reasonably well known (see JM88). The nuclei appear more elongated than small main-belt asteroids of comparable size, but there is no evidence for a difference in the mean rotation periods in this small observational sample. The elongation of the nuclei is so extreme that we are almost surprised not to have found any more nearly spherical nucleus among the five so far investigated.

c) Nucleus Density

The shape and the period together allow us to calculate a critical density ρ_c such that for $\rho < \rho_c$ the nucleus would be

TABLE V. Nucleus light-curve parameters.

UT Date	R [AU]	Δ [AU]	α [deg]	m_R[1]	Δm_R
1987 / Mar	3.99	3.16	9.0	13.8 ± 0.1	0.35 ± 0.10
1988 / Feb	2.37	1.95	24.1	14.3 ± 0.1	0.65 ± 0.05
1988 / Apr	2.09	1.24	19.4	14.3 ± 0.1	0.60 ± 0.05
1988 / Jun	1.63	0.77	28.0	14.3 ± 0.2	0.7 ± 0.1[2]

1 Mean absolute red magnitude
2 Corrected for coma contamination

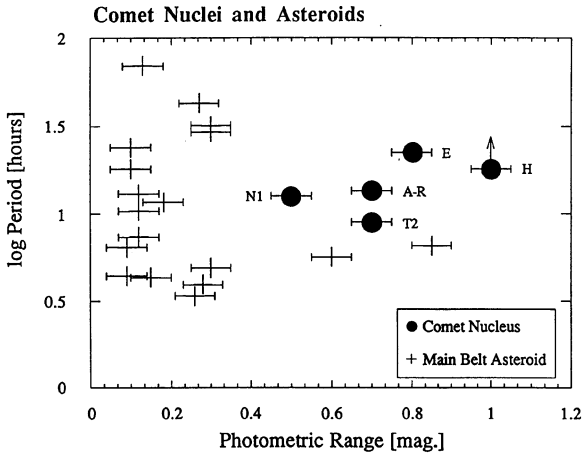

FIG. 13. Logarithm of the rotation period is plotted versus the photometric range, for a sample of well-observed cometary nuclei and small main-belt asteroids. The plotted nuclei are N1 = Neujmin 1, A–R = Arend–Rigaux, E = Encke, H = Halley, and T2 = Tempel 2. The rotation period of Halley is unknown—we have plotted a lower limit estimated from our own CCD photometry (see JM88).

in a state of internal tensile stress and would thus be unstable to centripetal disruption, while for $\rho > \rho_c$ the nucleus would be stable. By substitution into Eqs. (7) and (8) of JM88, we compute the critical density

$$\rho_c = 300 \text{ kg m}^{-3} . \quad (11)$$

We may regard ρ_c as an empirical lower limit to the bulk density of a monolithic prolate nucleus. For comparison, the least dense terrestrial snows have $\rho \approx 100$ kg m^{-3} (as any resident of a cold climate can show by melting a column of freshly fallen snow and comparing the depth of the melt to the thickness of the initial snow layer). Even with a 1:1 solid:ice mass mixing ratio, a nucleus structure analogous to that of light terrestrial snow would not satisfy Eq. (11). Thus, while Eq. (11) is by no means incompatible with Whipple's (1950) snowball model of the nucleus, it does suggest that the snow in the nucleus must be somewhat compact compared to fresh terrestrial snows. The inferred density limit is compatible with the revised fractal model of Donn and Meakin (1988), in which the density is $\rho \approx 600$ kg m^{-3}.

The density limit given in Eq. (11) is subject to uncertainty depending on the precise shape and spin state of the nucleus. The sense of the uncertainty, however, is to increase ρ_c (since we know only a lower limit to a:b). To take an extreme case, suppose that the nucleus is an undistorted contact binary. The measured period of rotation then constrains the density to be $\rho \geqslant 550$ kg m^{-3}, consistent with the limiting density ρ_c. Representing the nucleus as a Jacobi ellipsoid (Weidenschilling 1981), we also find $\rho > \rho_c$ so that, again, Eq. (11) gives a strong lower limit to the density. It is not impossible that the nucleus could have a significant tensile strength, but we consider this unlikely in the context of the agglomerated particle models of cometary nuclei (e.g., Donn and Hughes 1986). The propensity shown by many comets to split also attests to the low tensile strength of comet nuclei. Therefore, Eq. (11) is believed to provide a rather robust lower limit to the mean nucleus density. By comparison, the estimated density of the nucleus of P/Halley is rather uncertain, namely $\rho \approx 200$–1500 kg m^{-3} (Sagdeev, El'yasberg, and Moroz 1987). The latter density is based on estimates of the nucleus volume coupled with the measured nongravitational acceleration, and is obtained using a poorly constrained model of the angular distribution of the mass loss. Altogether, the centripetal method seems to provide a remarkably direct limit to the density of the nucleus of this comet.

d) Onset of Coma

We have seen from Fig. 12 that the appearance of a substantial coma in comet P/Tempel 2 was delayed until about 1988 April ($R \approx 2.1$ AU). Only in 1988 June ($R = 1.65$ AU) does the integrated light from the comet exceed the nucleus value by about 1 mag (Table IV). Why is substantial mass loss in Tempel 2 delayed until this remarkably small heliocentric distance? Water sublimation is certainly possible at larger heliocentric distances; indeed, water-driven activity in P/Halley began at $R \approx 6$ AU.

The appearance of the cometary dust coma coincides with the moment when the drag force on a grain due to gas flow through the nucleus surface becomes large enough to exceed the weight of the grain. We equate the drag and weight forces acting on a spherical grain of density ρ(kg m^{-3}), resting on the surface of a spherical nucleus of radius r_n and density ρ_n, to obtain the critical radius

$$a_{crit} = \frac{9 \mu m_H v Q}{64 G \pi^2 f r_n^3 \rho \rho_n} , \quad (12)$$

equal to the radius of a grain that can just be levitated by a given gas flow. In Eq. (8), $\mu = 18$ is the molecular weight of the gas, $m_H = 1.67 \times 10^{-27}$ kg is the mass of a hydrogen atom, v (m s^{-1}) is the gas velocity, Q (s^{-1}) is the total production rate of gas, and $f \leqslant 1$ is the fraction of the nucleus surface that actively sublimates. Equation (12) is a crude approximation in that it neglects the asphericity of the nucleus, the centripetal reduction in local gravity near the nuclear equator (which may be considerable), plus the nonradial gas flow near localized surface vents in the nucleus (Kitamura 1987).

The criterion in Eq. (12) suggests two general explanations for the delayed appearance of a coma. The first possibility is that the sublimation gas flow on Tempel 2 prior to 1988 May was unusually weak, so that the typical ≈ 1 μm diam coma grains could not be expelled. The second is that the grains on Tempel 2 are unusually large, so that an abnormally large gas flux is needed to produce a measurable dust coma.

Evidence against the "large grains" hypothesis is provided by the spatially and temporally resolved photometry in 1988 June. This photometry shows coma variations on timescales of hours, indicating that the coma grains are able to travel several $\times 10^6$ m in a time period of $\approx$ few $\times 10^4$ s. These 100 m s^{-1} grain speeds are just as expected for small (micron-sized) grains which couple well to the gas, but would be hard to reconcile with large grains. For this reason, we conclude that the gas flow from the nucleus was too weak to lift appreciable numbers of grains prior to about 1988 May. A natural explanation of the weak gas flow, and the delayed but rapid appearance of a coma, is in terms of shadowing or insulation of the near-surface ice in localized active areas on Tempel 2. Shadowing could be provided by a seasonal effect of the obliquity (Sekanina 1988a), while insulation by a refractory surface crust would be compatible with the low nucleus albedo and the known existence of such crusts on other nuclei. Evidence for a crust is described in Sec. V*e*.

e) Production Rates

The mass production rate of dust may be estimated from the continuum photometry in 1988 June as follows. The sum of the cross sections of the dust grains C (m^2) is related to the red magnitude of the coma (with the nucleus subtracted) by

$$p_R \phi(\alpha) C = 2.25 \times 10^{22} \ \pi R^2 \Delta^2 10^{0.4[m_R(\text{Sun}) - m_R]} , \quad (13)$$

where p_R is the dust geometric albedo, $\phi(\alpha)$ is the phase factor, $m_R(\text{Sun}) = -27.26$ is the magnitude of the Sun, and the other symbols are as previously defined (Russell 1916). In a power law size distribution $n(a)da \propto a^{-q} da$, the total mass of dust $\mathcal{M}$ (kg) is related to C by

$$\frac{\mathcal{M}}{C} = \frac{4}{3} \rho \frac{\int_{a_0}^{a_1} a^{3-q} da}{\int_{a_0}^{a_1} Q_s(a) a^{2-q} da} , \quad (14)$$

where ρ and a are the grain density and radius, q is the power law size index, and $Q_s(a)$ is the scattering efficiency of a grain of radius a (cf. Newburn and Spinrad 1985). The integrations extend over the size range $a_0 \leqslant a \leqslant a_1$. For simplicity, we rewrite Eq. (14) as

$$\mathscr{M} = \Psi \rho C, \quad (15)$$

where Ψ (m) is a numerical factor which must be computed for the particular size distribution assumed for the grains. The mass computed from Eqs. (13)–(15) is the mass of the observable grains released from the nucleus over one diaphragm-crossing time, defined simply by $\tau_d = P/v$, where P is the linear radial dimension of the projected photometry diaphragm or annulus, and v is the average grain-ejection speed. The dust mass production rate is then

$$\frac{d\mathscr{M}}{dt} = \frac{2.25\times10^{22}\,\pi\,\Psi\,\rho\,v\,R^2\,\Delta^2\,10^{0.4[m_R(\mathrm{Sun})-m_R]}}{p_R\phi(\alpha)P}. \quad (16)$$

Note that Eq. (16) gives a lower limit to the true dust mass production rate, since considerable mass could be contained within particles either too small ($a<0.1$ μm) or too large and therefore rare ($a>10$ μm), to be observed optically. Evidence that very large (millimeter sized) particles are ejected from P/Tempel 2 is provided by the *IRAS* dust trail associated with this comet (Sykes 1988).

Equation (16) was used to compute $d\mathscr{M}/dt$ from the m_R(2.5″–5.0″) mag in the 1988 June photometry. The quantity Ψ was estimated by setting $Q_s(a) = 1$, $a_0 = 0.1$ μm, and $a_1 = 10$ μm. For power law size distributions $q = 3.0$, 3.5, 4.0, 4.5, we obtain $\Psi = 2.9\times10^{-6}$, 1.3×10^{-6}, 0.6×10^{-6}, 0.4×10^{-6} (m). To an order of magnitude, then, we adopt $\Psi = 1\times10^{-6}$ (m) for the dust particles in P/Tempel 2. We adopt $p = 0.05$ and $\rho = 1000$ kg m^{-3} for the grains. The main uncertainty in $d\mathscr{M}/dt$ is due to the uncertain grain speed v, which we take to be the Bobrovnikoff speed for $R = 1.6$ AU, namely, $v_{BB} \approx 400$ m s^{-1}, and due to the mean grain size a, which we take to be $a = 10^{-6}$ m. Although the dust-production rates computed from Eq. (16) have a considerable absolute uncertainty, the relative uncertainties among the computed production rates should be small. The derived $d\mathscr{M}/dt$ are listed in Table VI.

The computed dust-production rates are of order 40–50 kg s^{-1}, and show only gradual variations with time in the 1988 June observing interval. For comparison we list published OH gas production rates for the 1988 June 10.4–July 28.3 interval. We believe that the gas-production rates in Table VI are as uncertain as the dust-production rates, because the gas-production rates refer to a symmetric model coma, whereas slit spectra show extreme asymmetry in the gaseous emissions from P/Tempel 2. Within the large uncertainties, we see from the table that P/Tempel 2 was losing mass at the rate of 40–400 kg s^{-1} in mid-June 1988, when at $R = 1.72$ AU. The measured rate of mass loss (40–400 kg s^{-1} in H_2O) can be supplied by equilibrium sublimation from an ice patch (albedo 0.03) of area 0.6–6 km^2, corresponding to about 0.15%–1.5% of the total surface area of the nucleus. The relative inactivity of P/Tempel 2 at a given R, compared to the similarly sized P/Halley, may therefore be ascribed to the smaller fraction of its surface area that is actively involved in sublimation.

TABLE VI. Mass-loss rates.

UT Date	Species	dM/dt [kg s^{-1}]	Reference
1988/06/10.4	OH	37	A'Hearn *et al.* 1988b
1988/06/11.5	OH	85	A'Hearn *et al.* 1988b
1988/06/11.5	CN	0.1	A'Hearn *et al.* 1988b
1988/06/11.5	C_2	0.1	A'Hearn *et al.* 1988b
1988/06/22	Dust	44	This Work
1988/06/23	Dust	43	This Work
1988/06/28.3	OH	398	Roettger *et al.* 1988
1988/06/30	Dust	50	This Work
1988/07/01	Dust	53	This Work

f) Surface Photometry: Fading Grains

The photometry from each of the $N \approx 90$ CCD images listed in Table IV can be used to construct a surface-brightness profile of the coma. Four of the 90 surface-brightness profiles of the comet in the red filter are plotted in Fig. 14. The profiles show the average surface brightness within each of the seven synthetic annuli, plotted versus the effective radius of each annulus. Also plotted on the figure are lines having logarithmic gradients $m = -1$ and $m = -1.5$. The physical significance of the $m = -1$ line is that it represents the surface-brightness profile of a steady-state, spherically symmetric coma. This simple model has been frequently used to represent the profiles of cometary comae. The $m = -1.5$ line represents the limiting case of a steady-state coma profile distorted by solar radiation pressure (Jewitt and Meech 1987, hereafter referred to as JM87).

The first observation to be made from Fig. 14 is that the

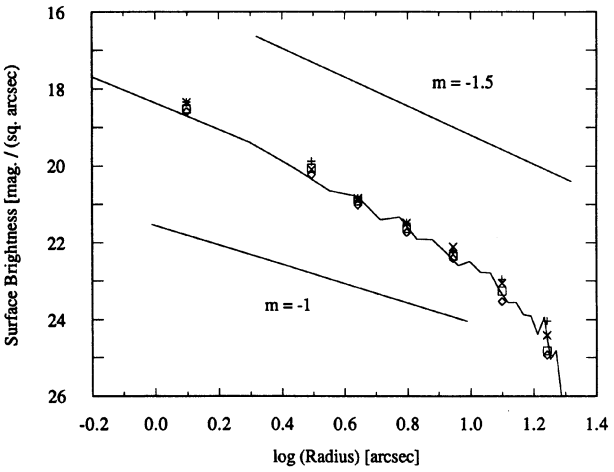

FIG. 14. Continuum surface-brightness profiles of comet P/Tempel 2, measured 1988 June 22 (+ marker), 23 (□ marker), 30 (○ marker), and July 1 (× marker). The upper and lower straight lines represent simplistic models of (a) a spherically symmetric, steady-state coma ($m = -1$) and (b) a radiation-pressure-dominated coma ($m = -1.5$). Neither model represents the P/Tempel 2 profile well. The curved line passing through the data is a Monte Carlo model of a coma in which the grains fade with increasing time of flight (see the text for details). The general agreement between the Monte Carlo model and the measured profiles supports the fading-grain hypothesis.

surface-brightness profiles taken in an eight night interval in 1988 June are very similar. There is no evidence for time-dependent effects which might be attributed to temporal modulation of the coma by the rotating nucleus. Therefore, we may assume that the measured surface-brightness profile is in steady state. The second observation to be made from Fig. 14 is that the coma surface-brightness profiles are steep compared to either of the model lines. The significance of this observation is that the coma cannot be interpreted using a simple model invoking only solar radiation pressure to explain the steep gradient. Specifically, radiation pressure cannot induce a surface-brightness gradient $m < -1.5$, and therefore it cannot readily account for the very steep gradient observed in the outer coma of P/Tempel 2. We note that the measurements of the surface-brightness profiles using concentric, circular annuli are legitimate, even though the coma does not exhibit circular symmetry (JM87).

What could be the cause of this steep surface-brightness profile? In the absence of any more convincing explanation, we interpret the Tempel 2 profile as indicating fading coma grains. The profile suggests that the grains decline in scattering cross section by a factor ~ 2 on distance scales 10″, corresponding to $\sim 10^4$ km at the comet.

What might cause the coma grains to fade? The obvious explanation, namely that fresh water-ice grains are sublimating under exposure to sunlight, is *not* viable. An exposed dirty water-ice grain would have an order-of-magnitude sublimation lifetime

$$t \approx \frac{4\rho a L R^2}{3 F_{\rm Sun}},$$

where $\rho = 10^3$ (kg m^{-3}) and a (m) are the grain density and radius, $L = 2 \times 10^6$ (J kg^{-1}) is the latent heat of sublimation, and $F_{\rm Sun} = 1360$ (W m^{-2}) is the solar constant. At $R = 1.6$ AU, the lifetime of a 10 μm grain would be of order 40 s, and the corresponding range $\ll 100$ km—this is small compared to the 10^4 km coma dimension. A detailed computation, including the effects of nongeometric optics, confirms that dirty water-ice grains should be confined to a halo about the nucleus no greater than a few hundred kilometers in radius, no matter what their initial size (e.g., Mukai *et al.* 1985).

A more appealing explanation of the steep profile is suggested by measurements of the coma of Comet Halley. There, collimated jets of CN and C_2 radicals suggest the presence of tiny sublimating organic grains (the "CHON" grains) in the coma (A'Hearn *et al.* 1986; Wallis, Rabilizirov, and Wickramasinghe 1987; Lamy and Perrin 1988). Furthermore, evidence for grain fragmentation was found from *in situ* measurements, and might be explained by electrostatic disruption (Boehnhardt and Fechtig 1987; Simpson *et al.* 1987) or by sublimation of interstitial organic binding material within an aggregate of many small particles. It is interesting to note that the surface-brightness profile of P/Halley at $R = 2.47$ AU was too steep to be accounted for by solar radiation pressure (JM87), consistent with the existence of sublimating and/or fragmenting grains in this comet (see Baum and Kreidl (1986) for other possible examples).

By analogy with comet P/Halley, then, we tentatively advance the hypothesis that the cause of the observed steep surface-brightness profile in P/Tempel 2 is the progressive destruction of organic grains, either by sublimation or fragmentation. The destruction of these grains is presumably the source of some fraction of the radicals observed in the coma. Indeed, this would provide a simple and natural explanation for the similarity of the spatial asymmetries of the gas and dust comae as witnessed by our CCD spectra. This explanation is also compatible with the relatively small production rates of the C_2 and CN radicals compared with dust (Table VI).

A quantitative demonstration of the fading-grain hypothesis was attempted using the Monte Carlo formalism described in JM87. We use a Monte Carlo program to produce a three-dimensional representation of the P/Tempel 2 coma, and then project the model onto the plane of the sky to simulate our CCD data. Photometry can be measured from the model in exactly the same way as from an astronomical CCD image.

The steps involved in the Monte Carlo model are briefly summarized in the Appendix. Several models were run with different particle-size distributions and radiation pressure and velocity scaling laws. All models had as input parameters the heliocentric and geocentric distance and the phase angle of comet P/Tempel 2 on 1988 June 22 (Table II). The particular model plotted with the data in Fig. 14 used an inverse-cube power law particle-size distribution, with minimum and maximum particle sizes $a_0 = 0.2$ μm and $a_1 = 10$ μm, respectively. The initial cross-section-weighted mean grain size of the particles in the distribution was $a_{\rm mean} = 2.5$ μm. The fading timescale for a grain of initial size $a_{\rm mean}$ was 10^5 s.

The measured surface brightness in the two inner apertures shown in Fig. 14 is higher than predicted by the model. This is the expected consequence of the nucleus, which is not modeled by the Monte Carlo program. The evident agreement between the observed and the model surface-brightness profiles in all other apertures in the figure is at least consistent with the hypothesis that the steep gradients in P/Tempel 2 are caused by fading grains. From the profile models alone, we cannot reach any conclusion about the physical process that causes the grains to fade (i.e., we cannot distinguish between sublimating and electrostatically fragmenting grains). However, the similarity between the 10^5 s fading timescale and the grain lifetime calculated for micron-sized organic grains by Lamy and Perrin (1988) is suggestive of sublimating organic grains.

g) Coma Waves

If the nucleus sublimation rate is periodically modulated by nucleus rotation, we should expect to see observable, periodic features in the coma. In particular, we expect that cyclic mass loss should drive a set of waves into the dust coma, with a speed equal to the cross-section-weighted phase speed of the coma-grain ensemble, and with an amplitude controlled by the velocity dispersion of the grains. Crudely, the minimal condition for the detection of these waves is $t_{\rm d} \leqslant t_{\rm n}$, where $t_{\rm d}$ is the time taken for a dust grain to cross the projected photometry aperture and $t_{\rm n}$ is the nuclear rotation period. For $t_{\rm d} \gg t_{\rm n}$, many successive waves are encompassed by the aperture, leading to a reduction in contrast and therefore in observability. The postulated waves have never been seen in the coma of any comet, perhaps because the above condition is rarely satisfied, but more likely because the waves have not been seriously sought. In P/Tempel 2, we know $t_{\rm n} = 8.95$ hr (3.2×10^4 s), and we estimate $t_{\rm d} \approx p/v$, where $p \approx 2 \times 10^6$ m is the linear radius of the 3.75″ synthetic photometry aperture and $v \approx 100$–400 m s^{-1} is the grain speed. We obtain $t_{\rm d} \approx 2 \times 10^4$–$5 \times 10^3$ s, which satisfies

$t_d \leqslant t_n$. Tempel 2 thus provides us with an excellent opportunity to search for coma waves.

The search for coma waves was done in the following way: the integrated magnitudes plotted in Fig. 8 were used to compute mean annular surface brightnesses within each of the seven photometric annuli. The surface brightnesses are plotted versus the time of observation in Fig. 15. This figure confirms that the largest photometric variations are confined to m_R (2.50″) (subtending 1400 km at the comet). A coma wave should appear in Fig. 15 as a ripple propagating from left to right. No such ripples are seen. Systematic variations *are* present in the coma apertures (especially m_R (2.50″–3.75″) and m_R (3.75″–5.00″)), but they are small compared with the central variations due to the rotating nucleus. The range of the systematic variations decreases with increasing annulus size, and the outermost apertures show no variations larger than the uncertainties of the photometry. No convincing evidence for waves, in the form of a time-lagged peak in the cross correlation, was found. Numerical experiments with time-dependent Monte Carlo models of dust comae suggest that the waves in Tempel 2 may easily be concealed by a large intrinsic velocity dispersion among the grains. Of course, it is also possible that the active areas on P/Tempel 2 were in perpetual sunlight at the time of observation, so that the diurnal modulation of sublimation would be greatly reduced.

h) Resolved Spectra of the Nucleus and Coma

The CCD reflectivities (Fig. 10(a)–(c)) can be used to extract the separate spectra of the nucleus and coma of P/Tempel 2. First, the central spectrum ((a) in Fig. 10) is recognized to contain emission from three sources, the nucleus, the dust coma, and the gas coma. The outer spectra, (b) and (c), contain emission from the dust and gas comae only. We estimate the nuclear contribution to spectrum (a) by interpolating the monochromatic surface-brightness profile in the spatial dimension across the central region containing the nucleus. The interpolation was done using a third-order polynomial fit to the coma in each pixel column along the dispersion axis of the CCD spectrum. The estimated fraction of the continuum signal in spectrum (a) in Fig. 10 due to coma is 25%–30%. Figure 16 shows the spectrum of the nucleus produced by subtracting the fitted coma component, together with a spectrum of the coma at slit position (b). As expected, the effect of the subtraction of the neutral coma is to slightly increase the reflectivity gradient of the nucleus above the value seen in spectrum (a). The gradient of the reflectivity of the coma-subtracted nucleus is $S' = 20\% \pm 3\%/1000$ Å. The gradient of the reflectivity of the cometary dust in slit position (b) is $S' = 1\% \pm 3\%/1000$ Å. These gradients correspond to $m_V - m_R$ colors 0.55 ± 0.03 and 0.36 ± 0.03, respectively, in the Kron–Cousins system (Fernie 1983).

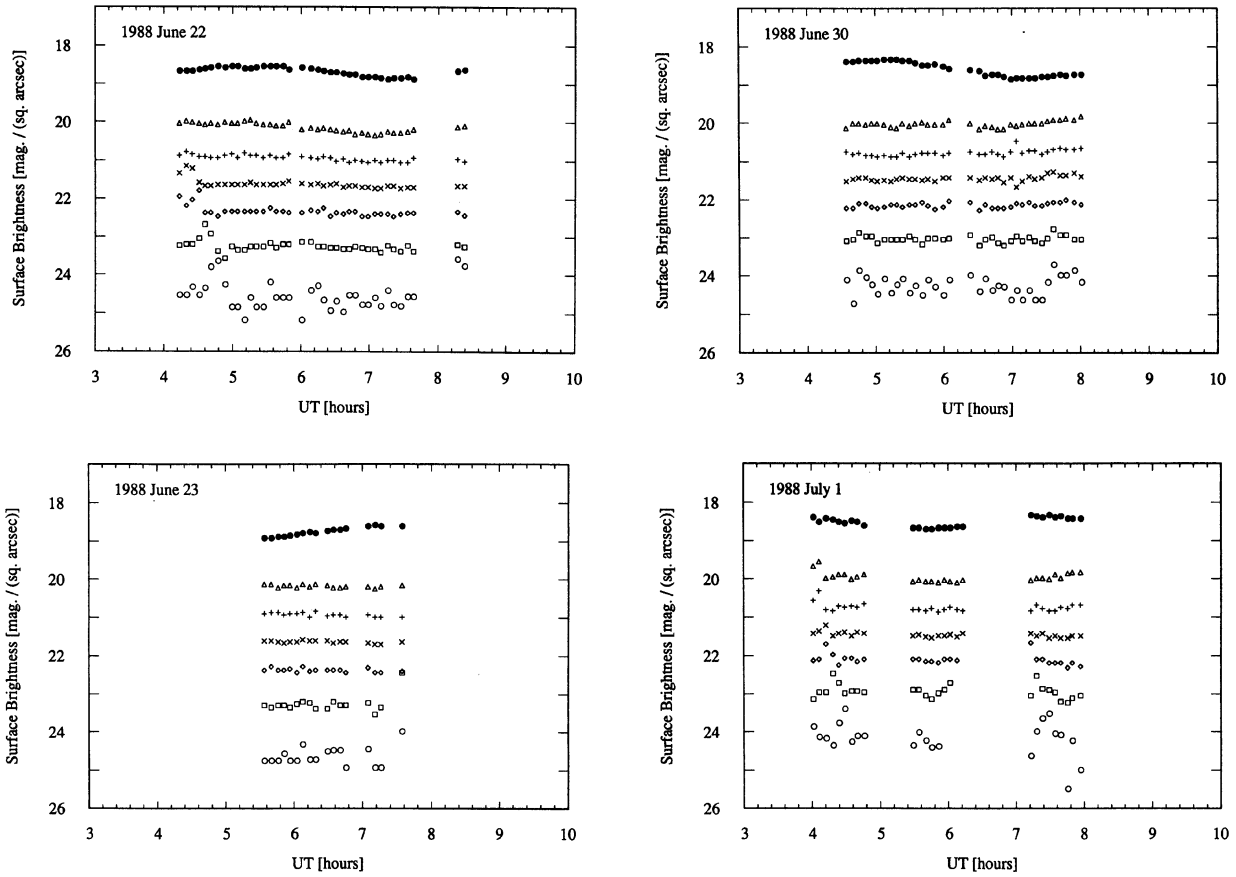

FIG. 15. Continuum surface-brightness measurements of P/Tempel 2 measured 1988 June 22, 23, 30, and July 1. The surface brightness (R filter magnitudes per square acrsecond) is plotted against the time of observation. The figure shows that the coma is nearly constant in surface brightness, except for the innermost annulus. Large photometric variations are confined to the inner (nuclear) aperture.

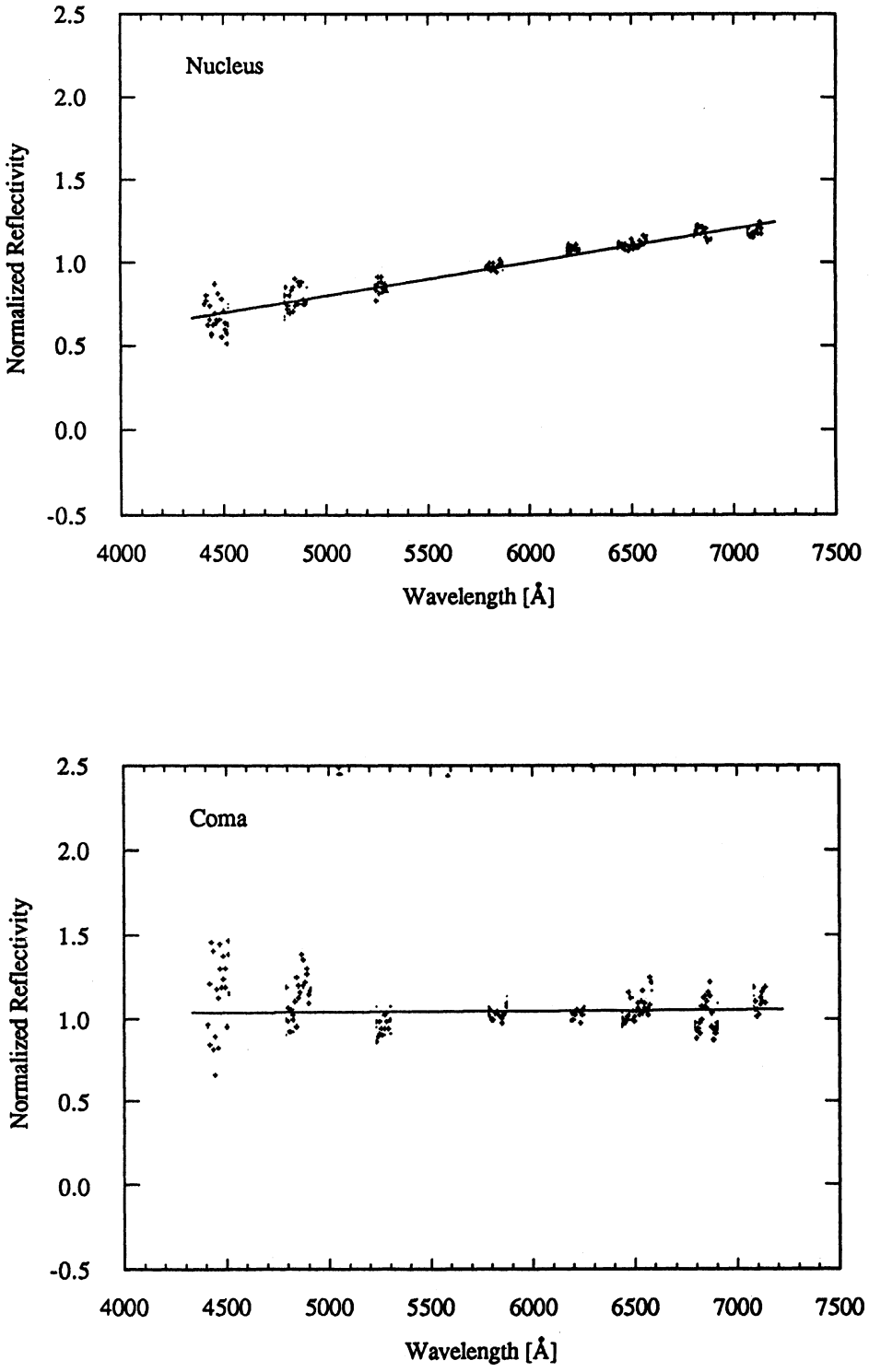

FIG. 16. Reflectivity spectrum of the nucleus of P/Tempel 2 normalized to unity at 5800 Å. The nucleus reflectivity has been obtained by correcting for a small amount of near-nucleus coma contamination, using the spatial information provided by the CCD spectrum. Wavelengths at which gas emission is known to occur have not been plotted. The straight line is a linear least-squares fit added to emphasize the linearity of the reflectivity. A decrease in the CCD quantum efficiency is responsible for the increased scatter in the data at short wavelengths.

The substantial redness of the nucleus is compatible with the $m_V - m_R$ broadband colors measured at about the same time as the spectra, and with $m_V - m_R$ colors measured in 1988 April at $R \approx 4$ AU (see Table VII). The agreement between colors determined using broadband filters on the one hand and CCD spectra on the other, and between colors measured near aphelion and near perihelion, is quite reassuring. The $S' = 20\% \pm 3\%/1000$ Å gradient is also consistent with the IIDS spectrum of Spinrad, Stauffer, and Newburn (1979) and with the multichannel-spectrometer data of Johnson, Smith, and Shorthill (1981). It is naturally tempting to compare the nucleus reflectivity spectrum (Fig. 16(a)) with the reflectivity spectra of known asteroid types. A broad resemblance to asteroids of types "S" and "D" is noticed. However, P/Tempel 2 cannot be regarded as type S, since its low albedo and large phase coefficient are absent in the high-albedo S type asteroids. The nucleus of comet P/Halley had $S' = 6\% \pm 3\%/1000$ Å (Thomas and Keller 1989), significantly less red than the nucleus of P/Tempel 2. Evidently, cometary nuclei exhibit different spectral characteristics.

We can find no unique explanation for the neutrality of the coma continuum, or for the color difference between the coma and the nucleus. The neutral coma continuum may be explained if the coma grains are small compared to the wavelength of light ($\lambda \approx 0.5$ μm), so that geometric scattering effects would be responsible for the color difference with respect to the nucleus. An alternative possibility is that the red color of the nucleus is produced by a radiation-damaged carbon-rich mantle, while the particles ejected into the coma have yet to suffer radiation damage, and so may have a different color. The color of the near-nucleus coma grains in P/Halley was similar to or slightly redder than the color of the nucleus (Thomas and Keller 1989). Sensible interpretation of the measured colors awaits a larger set of measurements of the spectra of cometary nuclei and their associated dust comae.

The gaseous emissions in Tempel 2 share the sunward asymmetry noted in the dust coma (Fig. 7). The magnitude of the asymmetry is sufficiently great that we would have little confidence in gas-production rates deduced by application of the traditional Haser model to our data. Therefore, we decline to present model production rates based on our spectra, at least until we have achieved a stronger understanding of the gas coma symmetry. Close examination of the gas emissions may provide independent evidence for the sublimation of coma grains, as inferred from the continuum surface-brightness profile in Sec. V*f*. These investigations will be the subject of a future paper.

TABLE VII. Color of P/Tempel 2.

UT Date	R [AU]	Δ [AU]	α [deg]	$m_V - m_R$[1] (mag)	S' % / 10^3 Å
1987 / Mar / 31 - 02	3.99	3.16	9.0	0.53 ± 0.03	18 ± 3[2]
1988 / Jun / 23	1.65	0.77	26.0	0.47 ± 0.05	12 ± 5[2]
1988 / Jun / 26	1.63	0.77	27.7	0.45 ± 0.02[3]	10 ± 2
1988 / Jun / 30	1.61	0.77	30.4	0.52 ± 0.05	17 ± 5[2]
1988 / Sep / 09[4]	1.39	0.92	46.6	0.55 ± 0.03[3]	20 ± 3

1 Color within 5" diameter diaphragm: in this system the solar color is $m_V - m_R = 0.35$.
2 S' computed from broadband measurement of $m_V - m_R$.
3 $m_V - m_R$ computed from spectrograph measurement of S'.
4 Corrected for coma contamination of the nucleus light.

VI. CONCLUSIONS

Time-series photometric measurements of comet P/Tempel 2 yield new, direct information about the physical properties of the nucleus, and about the properties of the coma surrounding this body. New findings concerning the *nucleus* include:

The synodic rotation period of the nucleus is $P = 8.95 \pm 0.01$ hr ($8^h 57^m 24^s \pm 36^s$). This is the shortest rotation period of any nucleus yet reliably measured.

The nucleus exhibits a 0.7 mag rotational variation, from which we infer that the nucleus is a prolate object (axes near $a:b:c = 1.9:1:1$). Elongated shape is a characteristic of all nuclei for which reliable shape determinations exist.

The bulk density of the nucleus must be $\rho \geqslant 300$ kg m^{-3}, if the material in the nucleus is not to be in a state of internal tensile stress.

The approximate absolute red magnitude of the nucleus is $m_R(1,1,0) = 14.3 \pm 0.1$ in 1988 photometry. Using an assumed albedo $p_R = 0.024$, we find that the approximate overall dimensions of the nucleus are $16 \times 8 \times 8$ km.

The nucleus of Comet Tempel 2 is reddened with respect to the Sun by $S' \approx 20\% \pm 3\%/1000$ Å; the optical reflectivity spectrum resembles the reflectivity spectra of S or D type asteroids in the wavelength range $4500 \leqslant \lambda \leqslant 7000$ Å; the spectrum and low albedo together suggest a closer similarity to asteroid type D.

New findings concerning the *coma* include:

Measurable mass loss from Tempel 2 began remarkably late in the approach to perihelion, at the small heliocentric distance $R \approx 2$–2.5 AU. Near-surface water ice was shielded from sunlight prior to this time, perhaps by an insulating crust, or more likely by shadowing due to the nucleus obliquity.

The comet is only weakly active at $R = 1.6$ AU. The mass-loss rate in solids (40–400 kg s^{-1}) can be sustained by sublimation from water ice occupying only 0.15%–1.5% of the surface area of the nucleus.

The surface-brightness profile of the dust coma is too steep to be described by simple radiation-pressure models of the kind that apply to a majority of comets measured to date. The profile provides strong evidence for fading of the coma grains with increasing distance from the nucleus. The fading may be due to the progressive destruction of CHON grains by the loss of volatiles under solar irradiation.

The coma dust grains are nearly neutral scatterers, in contrast to the reddened nucleus.

Dramatic photometric variations due to the rotation of the nucleus of P/Tempel 2 are muted or absent in most of the coma. The photometrically inert appearance of the coma may be explained by a wide velocity dispersion among the coma particles released from the nucleus. Rotational modulation of the coma as seen in comet P/Halley is apparently absent in comet P/Tempel 2.

We thank Matt Johns, Bob Barr, and Larry Breuer for support of the equipment at McGraw–Hill Observatory, and

Gerry Luppino for help with the Big Red Imaging CCD Camera. We especially thank Bob Barr for emergency repair of a catastrophic dome problem. This work was supported in part by grants from NASA and the NSF to D. C. J., and by a NASA Graduate Student Researcher Award to J. X. L.

APPENDIX

The Monte Carlo algorithm described in Sec. V*f* included the following steps.

(1) Select a particle diameter from an assumed power law size distribution.

(2) Compute the particle ejection speed based on the particle diameter.

(3) Emit the particle in a randomly selected direction from a point-source nucleus located at the origin of a Cartesian coordinate system.

(4) Accelerate the particle in the antisolar direction to reproduce the effect of solar radiation pressure. The magnitude of the acceleration is computed from the size of the particle and an assumed radiation-pressure law.

(5) Allow the radius of the particle to decrease in proportion to the time of flight, to simulate the fading of the grains.

(6) Compute and store the Cartesian coordinates and the radius of the particle after the time of flight.

(7) Project the x,y,z coordinates of each particle onto a plane oriented inclined to the Sun–comet line by an angle equal to the actual phase angle of observation.

(8) Repeat steps (1)–(7) for each of 10^5 particles.

(9) Do photometry on the projected particles, for comparison with CCD data.

REFERENCES

A'Hearn, M. F., Campins, H., and Schleicher, D. (1988a). IAU Circ. No. 4614.
A'Hearn, M. F., Feldman, P., Roettger, E., and Schleicher, D. (1988b). IAU Circ. No. 4622.
A'Hearn, M. F., Hoban, S., Birch, P. V., Bowers, C., Martin, R., and Klinglesmith, D. A. (1986). Nature **324**, 649.
Barker, E. S., Cochran, A. L., and Rybski, P. M. (1981). In *Modern Observational Techniques for Comets*, JPL Publ. No. 81-68 (JPL, Pasadena).
Baum, W. A., and Kreidl, T. J. (1986). In *Asteroids, Comets, Meteors II*, edited by C. I. Lagerkvist, B. A. Lindblad, H. Lundstedt, and H. Rickman (Uppsala University, Uppsala), p. 397.
Boehnhardt, H., and Fechtig, H. (1987). Astron. Astrophys. **187**, 824.
Christian, C. A., Adams, M., Barnes, J. V., Butcher, H., Hayes, D. S., Mould, J. R., and Siegel, M. (1985). Publ. Astron. Soc. Pac. **97**, 363.
Donn, B., and Hughes, D. (1986). In *Proceedings of the 20th ESLAB Symposium on the Exploration of Halley's Comet*, Heidelberg, ESA SP-250 (ESA, Noordwijk).
Donn, B., and Meakin, P. (1988). Bull. Am. Astron. Soc. **20**, 840.
Dworetsky, M. M. (1983). Mon. Not. R. Astron. Soc. **203**, 917.
Fernie, J. D. (1983). Publ. Astron. Soc. Pac. **95**, 782.
Goldstein, R. M., Jurgens, R. F., and Sekanina, Z. (1984). Astron. J. **89**, 1745.
Jewitt, D. C., and Luu, J. X. (1988). IAU Circ. No. 4582.
Jewitt, D. C., and Meech, K. J. (1987). Astrophys. J. **317**, 992.
Jewitt, D. C., and Meech, K. J. (1988). Astrophys. J. **328**, 974.
Johnson, P. E., Smith, D. W., and Shorthill, R. W. (1981). Nature **289**, 155.
Kamoun, P. D., Campbell, D. B., Ostro, S. J., Pettengill, G. H., and Shapiro, I. I. (1982). Science **216**, 293.
Keller, H. U., Delamere, W. A., Huebner, W. F., Reitsema, H. J., Schmidt, H. U., Whipple, F. L., Wilhelm, K., Curdt, W., Kramm, R., Thomas, N., Arpigny, C., Barbieri, C., Bonnet, R. M., Cazes, S., Coradini, M., Cosmovici, C. B., Hughes, D. W., Jamar, C., Malaise, D., Schmidt, K., Schmidt, W. K. H., and Seige, P. (1987). Astron. Astrophys. **187**, 807.
Kitamura, Y. (1987). Icarus **72**, 555.
Lamy, P. L., and Perrin, J-M. (1988). Icarus **76**, 100.
Millis, R. L., and Sleicher, D. G. (1986). Nature **324**, 646.
Mukai, T., Mukai, S., Fechtig, H., Grun, E., and Giese, R. H. (1985). Adv. Space Res. **5**, 339.
Newburn, R. L., Jr., and Spinrad, H. (1985). Astron. J. **90**, 2591.
Oke, J. B. (1974). Astrophys. J. Suppl. **27**, 21.
Roettger, E. E., Feldman, P. D., A'Hearn, M. F., and Festou, M. C. (1988). Bull. Am. Astron. Soc. **20**, 819.
Russell, H. N. (1916). Astrophys. J. **43**, 173.
Sagdeev, R. Z., El'yasberg, P. E., and Moroz, V. I. (1987). Sov. Astron. Lett. **13**, 259.
Sekanina, Z. (1987). ESA SP-278 (ESA, Noordwijk), p. 323.
Sekanina, Z. (1988a). IAU Circ. No. 4553.
Sekanina, Z. (1988b). IAU Circ. No. 4624.
Simpson, J. A., Rabinowitz, D., Tuzzolino, A. J., Ksanfomality, L. V., and Sagdeev, R. Z. (1987). Astron. Astrophys. **187**, 742.
Spinrad, H., Stauffer, J., and Newburn, R. L. (1979). Publ. Astron. Soc. Pac. **92**, 707.
Stone, R. P. S. (1977). Astrophys. J. **218**, 767.
Sykes, M. V. (1988). Astrophys. J. Lett. **334**, L55.
Tedesco, E. F., and Barker, E. S. (1981). In *Comets: Gases, Ices, Grains and Plasma*, IAU Colloquium No. 61 (University of Arizona, Tucson).
Thomas, N., and Keller, H. U. (1989). Astron. Astrophys. (in press).
Wallis, M. K., Rabilizirov, R., and Wickramasinghe, N. C. (1987). Astron. Astrophys. **187**, 801.
Weidenschilling, S. J. (1981). Icarus **46**, 124.
Whipple, F. L. (1982). In *Comets*, edited by L. L. Wilkening (University of Arizona, Tucson), pp. 227–250.
Wisniewski, W. (1988). IAU Circ. No. 4603.

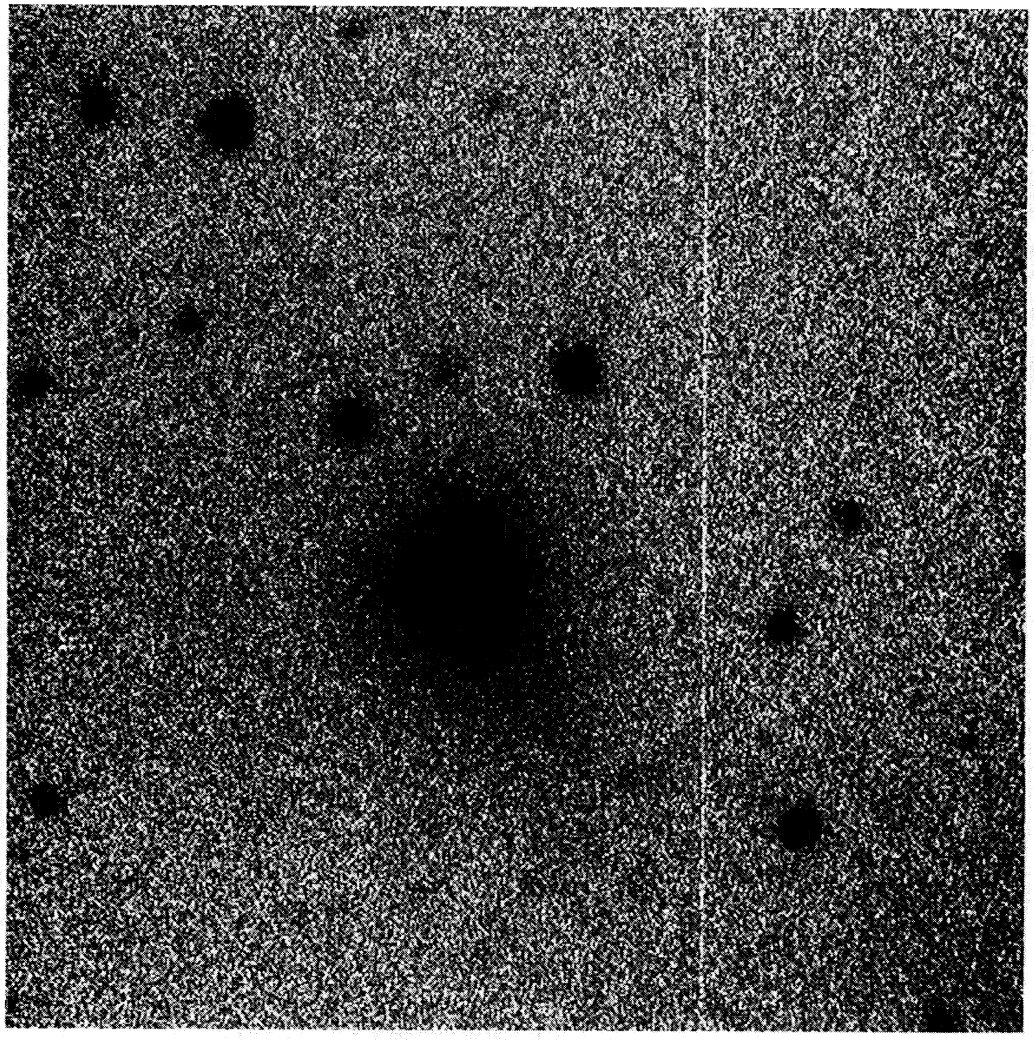

FIG. 6. Charge-coupled-device image of comet P/Tempel 2 taken 1988 June 22 05^h 05^m ($R = 1.65$ AU). The image is a 300 s red integration taken at the 2.4 m telescope. An asymmetric coma is clearly apparent. The field of view shown is 125″ on a side. North is to the top, east to the right.

D. Jewitt and J. Luu (see page 1769)

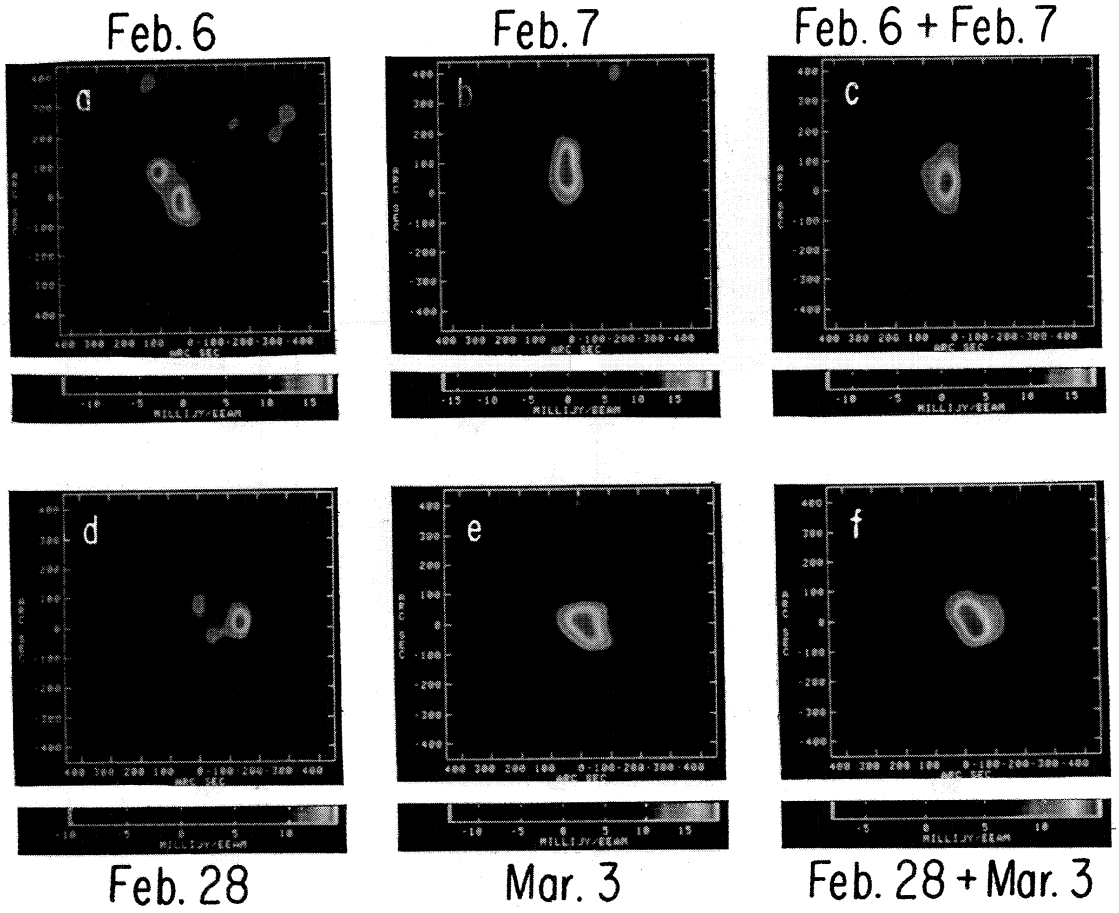

FIG. 2. False-color images of the velocity-averaged OH emission. Panel (a) is for February 6; (b) February 7; (c) the average of February 6 and 7; (d) February 28; (e) March 3; and (f) the average of February 28 and March 3.

Palmer *et al.* (see page 1792)